2015

Synthesis and Photophysical Study of Ruthenium Complexes

Shyam R. Pokhrel

Synthesis and Photophysical Study of Ruthenium Complexes

By

Shyam Raj Pokhrel

Thesis

Presented in Partial Fulfillment of the requirements for the degree of

Masters in Science, in Inorganic Chemistry

The University of Montana

Missoula, MT

Summer 2015

Approved by:

Dr. Edward Rosenberg Committee Chair

Department of Chemistry

Dr. Chuck Thompson Committee Member

Biomedical and Pharmaceutical Sciences

Dr. Orion Berryman

Department of Chemistry

Abstract

Selected ruthenium complexes with general formula [Ru(CO)(TFA)(PPh_3)$_2$(ppy-R)][(where ppy = 2, phenylpyridine (**1a**) and 2–(p–tolyl)pyridine (**1b**)], [Ru($PPhMe_2$)$_2$(CO)$_2$(TFA)$_2$] (**2**), [Ru(CO)(L)($PPhMe_2$)$_2$(bpy-R)]$^+$[PF_6]$^-$ [where bpy = 2,2′–bipyridyl, L = TFA, R = H (**3a**), L = H, R = H (**3b**) and L= H, R= Me at 4,4'-position of bipyridyl ligand (**3c**)] have been synthesized, characterized, and the photophysical properties were measured. Compound **2** was used as a starting material for the synthesis of photo-luminescent complexes (**3a**), (**3b**), (**3c**), (**3d** and **3d′**). The luminescent complexes **3d** and **3d′** with formula [Ru($PPhMe_2$)$_2$(CO)(H)(4–methyl, 4′-bromomethyl, 2,2′–bipyridyl)]$^+$[PF_6]$^-$ were derived by brominating one of the methyl group of 4,4′–dimethyl-2,2′–bipyridyl ligand. Newly synthesized isomeric species **3d** and **3d′** were loaded on a silica polyamine composite to measure their photophysical behavior in the solid environment. The successful loading of complexes on silica surface is expected to broaden the possibility of their application as heterogeneous catalysts in photochemical reactions.

Acknowledgements

First and foremost, I would like to express my deepest gratitude to my research advisor, Professor Edward Rosenberg. It was my wonderful opportunity to join his research group for my graduate studies. His continuous guidance, advice and limitless patience over a period of three years have been unbelievably helpful to broaden my knowledge and skill in chemistry. Thank you so much for your time, guidance, and encouragements! I would also like to thank to my committee member Professor Chuck Thompson and Professor Orion Berryman for their valuable inputs throughout my research.

Similarly, I would like to thank Professor Alexander Sandy Ross for his time and help in measuring the photophysical properties of my complexes despite his busy schedule. My sincere thanks also go to Michelle Terwilliger for her valuable guidelines to study the photophysical behavior of my complexes. I would like to thank my colleague, Daniel Decato, for his work on single crystal X-ray characterization of all my complexes. Similarly, I am grateful for the help Dr. Geoffrey Abbott who instructed me on electrochemistry and other chemical phenomena.

I would like to acknowledge my lab-mate, Abdul Goni who has helped me in routine laboratory activities. Similarly, I would like to thank Dr. John Hoody for his help in chromatographic separation and GC-Ms characterization of my compounds.

At last, I would like to express my sincere gratitude to my parents for everything they have given in my life without any expectation of return. My appreciation goes to my siblings for their continuous support and encouragements in my academic pursuits. My endless appreciation goes to my life partner- Prakriti, sons – Swarnim and Saurav for standing on my side for my successful graduate studies.

Contents

List of Figures

Lists of Tables, Charts and Schemes

List of Abbreviations

AA	Atomic Absorption
Abs.	Absorption
bpy	2,2′-bipyridine
bpy-Br	4−methyl−4′−bromomethyl−2,2′-bipyridyl
BP−1	Polyallylamine Coated Particles
DCM	Dichloromethane
DI	De−Ionized Water
DIPEA	N,N-Diisopropylethylamine
DNA	Deoxyribonucleic Acid
FTIR	Fourier Transform Infrared Spectroscopy
HOMO	Highly Occupied Molecular Orbital
IR	Infrared
KBr	Potassium Bromide
KHz	Kilohertz
LC	Ligand Centered
LFSE	Ligand Field Stabilization Energy
LLCT	Ligand to Ligand Charge Transfer
LUMO	Lowest Unoccupied Molecular Orbital
MC	Metal Centered
MLCT	Metal to Ligand Charge Transfer
MHz	Megahertz

NMR	Nuclear Magnetic Resonance
ORTEP	Oak Ridge Thermal Ellipsoid Plot
Phen	1,10−phenanthroline
ppy	2−phenylpyridine
SPC	Silica Polyamine Composite
TCSPC	Time Correlated Single Photon Counting
TFA	Trifluoroacetic Acid
THF	Tetrahydrofuran
TLC	Thin Layer Chromatography
tpy	terpyridine
UV	Ultraviolet

Introduction

The photochemistry of transition metal complexes has played an important role over past few decades especially in photonic and optoelectronic devices [1]. Among them, ruthenium complexes with different chelating ligands such as 2,2′–bipyridine (bpy), 2–phenylpyridine (ppy), 1,10–phenanthroline (phen), 2,2′:6′,2”–terpyridine (tpy), etc. and their hundreds of derivatives have attracted the attention of many chemists. Specific combinations of redox properties [2], quantum yield, longer excited–state lifetimes, longer luminescence and photostability [2,3] are some of the attractive features of these compounds. Utilizing these properties, solar energy conversion devices such as Gratzel cells [4] and other semiconductor devices [5] have been developed. Complexes with π–acid ligands have also been used as photocatalysts [6] for the oxidation of water [7], the production of hydrogen [8], optical sensors of pH [9] and the detection of cations and anions [10,11]. Further, the luminescent complexes of ruthenium have been reported as probes for immunoassay and the study of biomolecules like DNA [12], lipids, cholesterol [13] and proteins [14].

With the chelating ligands such as bpy or ppy, divalent ruthenium exists in a low spin d^6 electronic system where the chelating ligands act as a strong σ–donors through nitrogen or carbon and as π–acceptor ligands through delocalized orbitals of the aromatic rings. Among the prototypical bipyridine complexes, $[Ru(bpy)_3]^{2+}$ is the most studied compound possessing D_3 symmetry. It exhibits three types of molecular orbitals mostly contributed from ligands [15]: one σ–bonding and two π–bonding. The σ–bonding molecular orbital results from the head–on overlap between metal and ligand orbitals with appropriate symmetries and they are represented

by σ_L. Similarly, π_L and π_L^* molecular orbitals are formed by the side–by–side overlap of metal d–orbitals with the ligand π–orbitals of appropriate symmetry and the ligands are the major contributors to bonding electrons. Similarly the other two sets of orbitals on these octahedral complexes are π_M and σ^*_M which are developed by a degenerate t_{2g} and e_g set of d–orbitals on the central metal ion. Under usual circumstances, the π_L and σ_L molecular orbitals of the complexes are completely filled with their ground state electronic configurations, while they are partially filled with metal centered π_M orbitals, depending upon the availability of d-orbital electrons.

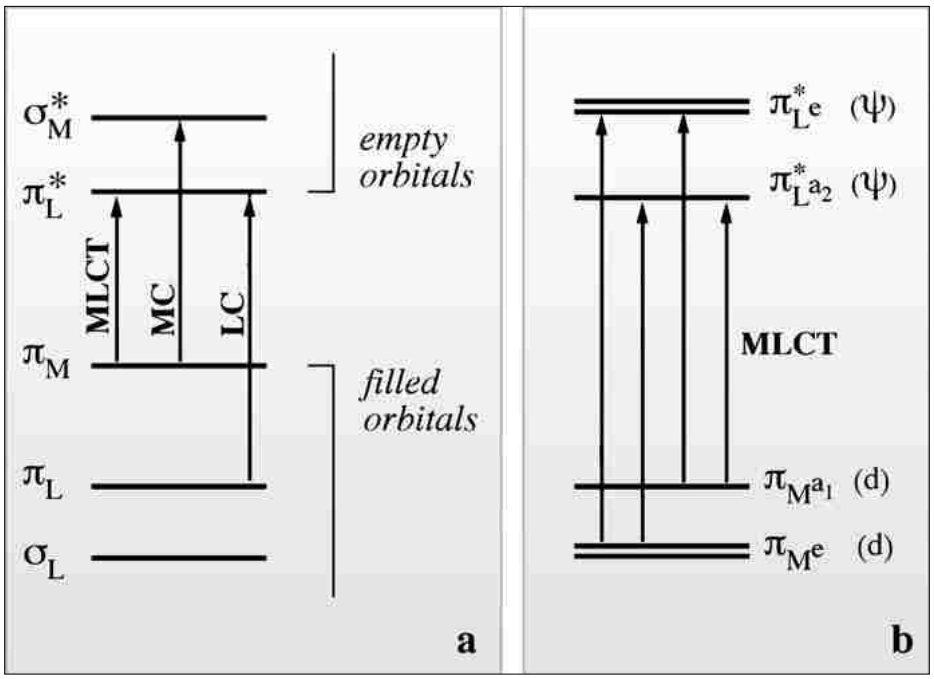

Fig. 1 (a) Simplified M.O. diagram for Ru(II) polypyridine complexes in octahedral symmetry; (**b**) **R**epresentation of the MLCT transition in D_3 symmetry [15]

Considering the single electronic configuration between the ground and the excited states in such octahedral complexes, there will be three types of possible electronic transitions *viz.*

metal–to–ligand ($\pi_M \rightarrow \pi_L^*$) charge transfer (MLCT) transition, metal–to–metal charge transfer transition ($\pi_M \rightarrow \sigma_M^*$) and ligand–to–ligand ($\pi_L \rightarrow \pi_L^*$) charge transfer (LLCT) transition (Fig. 1a). The low–energy MLCT transition is generally observed in the visible region, while the high–energy LLCT is observed in the UV–region of the electromagnetic spectrum [16]. Regardless of the nature of the excited state, the spin multiplicity of the Ru–complexes is either singlet (↑↓) or triplet (↑↑). These spin states undergo mixing between metal–centered (MC) and MLCT excited states due to the more favorable spin −orbit coupling [17–20].

In terms of symmetry, $\pi_M a_1(d)$ and $\pi_M e(d)$ orbitals (the ground state electronic configuration of the complex in its singlet state) represent the highest occupied metal–based molecular orbital (HOMO), and the $\pi^*_L a_2(\psi)$ and $\pi^*_L e(\psi)$ represent the lowest unoccupied ligand–based molecular orbitals (LUMO) (Fig. 1b) [21–23]. When the ligand field stabilization energy (LFSE) is sufficiently high, the ligand undergoes reduction by the metal electrons. However, when the LFSE is low, the ligand reduction is omitted due to the weak field nature of the ligand. In the former case, the metal complex might be fundamentally applicable to luminescence, while in the latter case, it can undergo either radiationless decay to the ground state or the ligand dissociation reaction. As a result, there is a very short excited state lifetime of the transition state and no luminescence is observed [18, 24, 25].

In ruthenium d^6 octahedral complexes, though MC excited states are strongly displayed while the ligand–centered (LC) and MLCT excited states are not strongly displayed relative to the ground state geometry, as shown in Fig. 2.

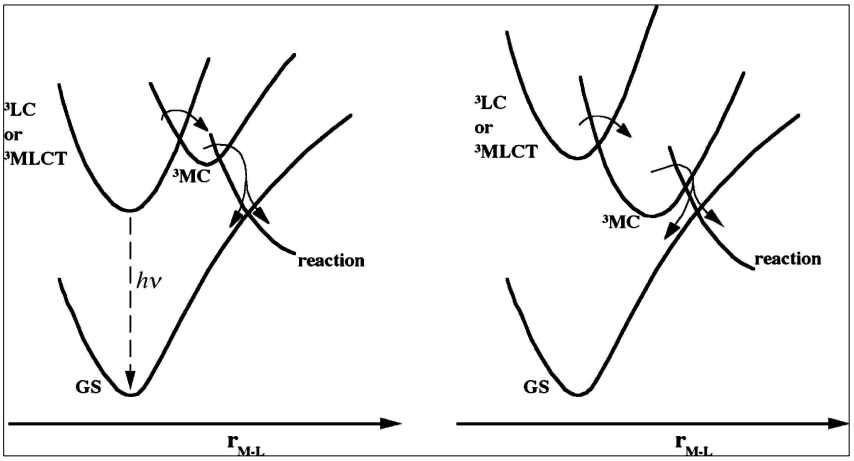

Fig. 2 Schematic representation of relative positions of ^{3}MC and ^{3}LC or (^{3}MLCT) excited states [25]

Since the excited triplet ^{3}MLCT has a higher degree of spin–orbit coupling, the rate constant for radiative deactivation for ^{3}MLCT is higher than that of ^{3}LC. Consequently, the ^{3}MLCT excited state will have a higher luminescence in fluid solution even at room temperature, while the ^{3}LC excited state will have a longer lifetime in a rigid matrix only at a low temperature [25]. The energy of MLCT, MC and LC in their excited state is determined by the redox properties of metal and ligands, ligand field strength and the intrinsic properties of ligands respectively (Figure 3).

For a number of analogous complexes with the same metal ion, the energy level especially the one with lowest orbital energy in an excited state can be controlled by choosing the suitable ligand [24–27]. In this way, the complexes with some expected properties can be developed by tuning the electronic properties of the ligands.

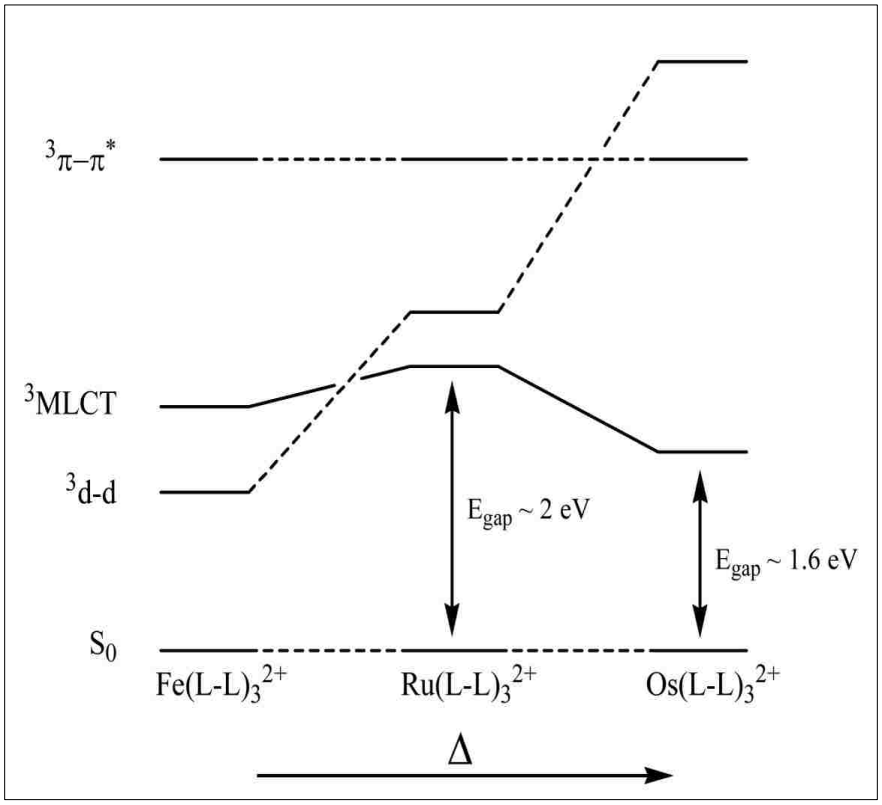

Fig. 3 Lowest energy triplet states for metal–ligand complexes with increasing crystal field strength [28].

Even all the complexes, formed from the different transition metals of the same group in the periodic table are not equally luminescent because they will have to fulfill the some specific criteria. As shown in Fig. 3, for better luminescence of the complex, the ligand field must be strong enough to shift its d–d level above the MLCT state. This specific property is found only in Ru^{2+} but not in Os^{2+} and Fe^{2+} ion. In the case of $[Fe(L–L)_3]^{2+}$ ions (where L = diimine ligands such as 2,2′–bipyridyl and 1,10–phenanthroline along with their derivatives), the ligand field is not sufficiently strong enough to split e_g–t_{2g} set of d–orbitals, while in the case of the Os^{2+} ion, the energy of the excited triplet state is almost equal to the ground state.' Hence, the $[Fe(L–L)_3]^{2+}$ complexes undergo radiationless decay while the corresponding Ru^{2+} and Os^{2+} complexes show a very strong luminescence [28].

Relative to other 4d–transition metals, the Ru(II) ion is a more convenient precursor for making chelating luminescent complexes with bpy, ppy and their derivatives. Although both series of ligands undergo complexation with the electrophilic metal center, the bpy forms two dative bonds through the lone pairs on each nitrogen atoms while the ppy forms an additional covalent bond through the carbon located at ortho position to the point of attachment to the pyridyl ring. This results in the formation of five–membered chelate ring, structurally similar to complexes with bipyridal ring system but has one carbanion resulting after the deprotonation of phenyl ring. This negatively charged carbon has more σ–donating ability to the metal center [29].

From the beginning, our group has been interested in synthesis and surface modification of silica polyamine composites (SPC), a highly cross-linked polymer made up of silica and polyamines. The composite material acts as a heterogeneous surface that is relatively easy to modify, and can be synthesized on salinized silica gel by using a range of polyamines [30]. After such modification on amorphous silica, SPC increases its higher surface stability and absorptivity which are desirable features in the separation science. Such properties of these materials have long been used for the removal of Co^{2+}, Ni^{2+} and Cu^{2+} ions from aqueous solution [31]. In addition, our groups has successfully loaded a set of transition metal complexes of Ru(III), Rh(III) and Pd(II) on the SPC surface, and used them as heterogeneous catalysts for the selective hydrogenation of different olefin and diene molecules. These metal loaded SPC materials have exhibited higher catalytic efficiency and turnover frequencies in comparison to the conventional heterogeneous hydrogenation catalysts [32].

These interesting properties of silica polyamine composite (SPC) prompted us to study the photo-physical properties of Ru (II) complexes conjugated on the silica surfaces. Therefore,

we designed the new Ru(II) complexes with suitable tethering groups (Chart 1) that exhibit higher reactivity towards amine functionality of SPC.

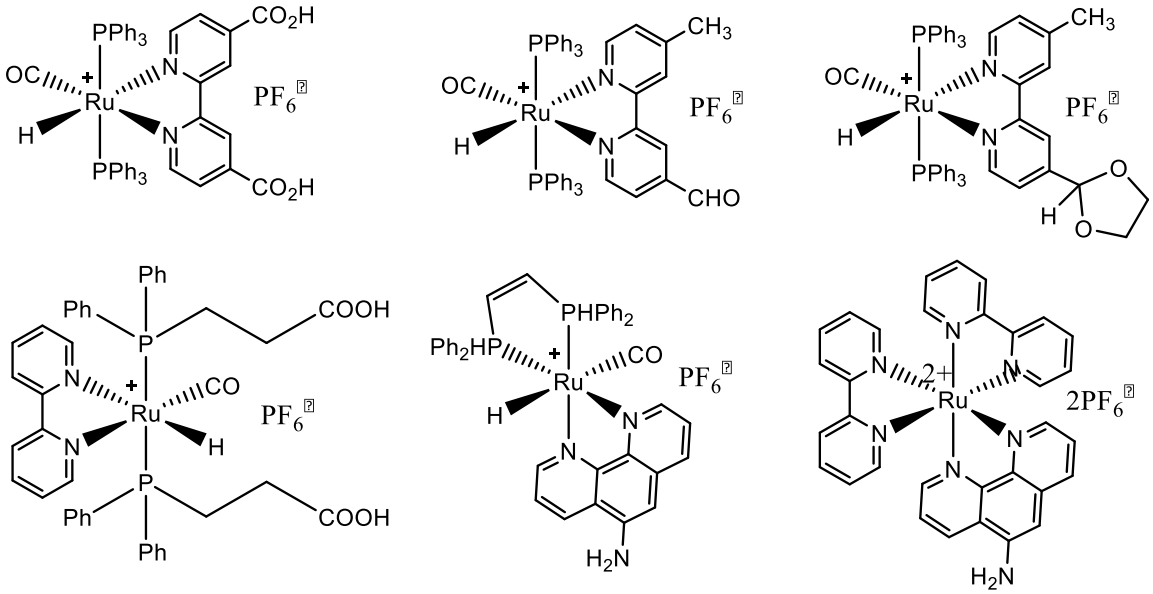

Chart 1. Structures of the ruthenium complexes studied.

The loading of metal complexes on composite materials was assessed by Atomic Absorption Spectroscopy (AAS) which showed the loading up to 3% based on the mmol of N per gram of BP-1. After the successful loading and characterization of these photo-stable Ru(II) complexes on SPC (BP-1 and WP-1) surface, we were able to measure their absorption-emission spectra and their excited state lifetime. When the complexes were covalently immobilized on the surface of silica polyamine composites (Chart 2), the excited state lifetimes of bound complexes were found to be 1.4 to 8 times longer than the unbound complexes in solution [33].

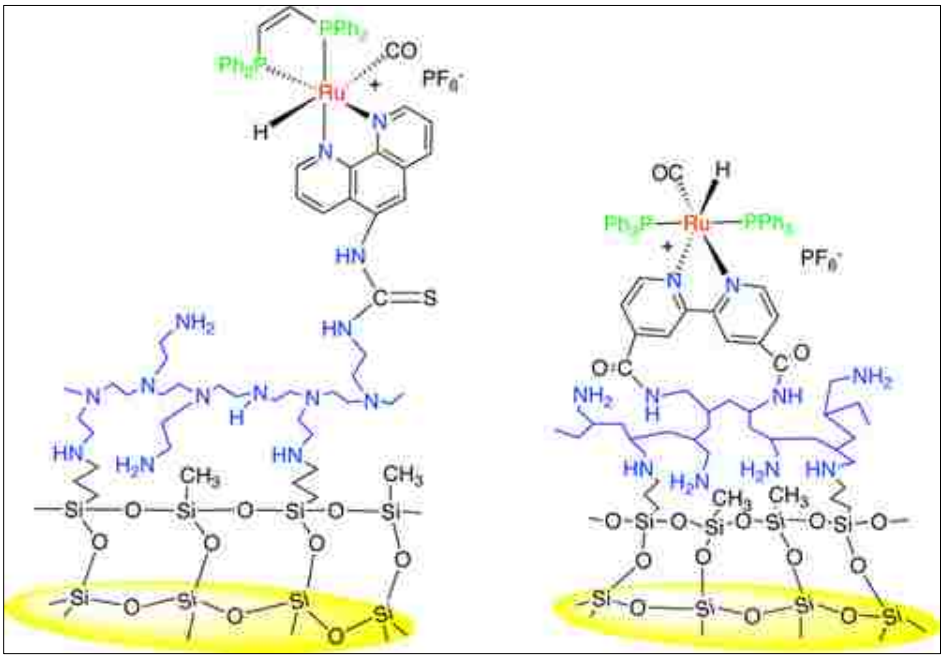

Chart 2. Covalently immobilized ruthenium complexes in silica polyamine composites.

The excited state lifetime of the complexes is also related to molecular volume and number of steric interactions with surface. Rigidity and mobility of complex molecules on the surface are other factors that determine the excited state lifetime. Electronic delocalization in the excited states is additional factor related to the luminescent properties of the complexes in the solution. Longer excited state lifetimes have a remarkable effect on lowering energy of activation for electron transfer reaction relative to other ruthenium diimine complexes. As such, higher air stability and durable luminosity of the surface bound complexes have opened the door for detail investigation of the electron transfer properties in heterogeneous environment [33].

In this context, we decided to further our research to investigate the photo-luminescent behavior of new ruthenium complexes in heterogeneous environment of SPC material and developed two sets of analogous complexes containing 2–phenylpyridine (ppy-R) and 2,2′–bipyridine (bpy-R) ligands. With the cyclometallated ppy-R ligand, we have used the bulkier triphenylphosphine (PPh_3) groups on *trans*–position to each other. However, with bpy-R series we have used less steric and better σ–donating dimethylphenylphosphine ($PPhMe_2$) ligands in their *trans*–positions. The ruthenium complexes synthesized with ppy-R groups only give the luminescence in blue −shifted region (400 nm) while those synthesized with bpy-R ligands showed in red −shifted region (600 nm). Although both sets of complexes successfully worked as a model and provided a valuable idea to further our research, our study was mainly oriented to develop the complexes that give bathochromic (red–shifted) luminescence and their behavior on the SPC surface. Therefore, we have developed a second set of compounds (ruthenium complexes having 2,2′–bipyridyl ligand) with suitable anchoring group for covalent binding to the SPC surface. Since the methyl side chain provides an opportunity of attaching the complex with silica polyamine composite (BP-1) following bromination, we have selectively brominated one of the methyl groups of 4,4′–dimethyl–2,2′–bipyridyl ligand. As bromine is a good leaving group; complex would easily conjugate on the composite surface after its removal and would give the better percentage of loading relative to the previously used anchoring groups such as –NH_2, -COOH, -CHO etc. Likewise, we thought that loading of complexes on the composite surface is also determined by the steric environment of other ligands. For example, in the previously synthesized Ru-complexes, mostly the highly steric triphenylphosphine (PPh_3) ligand have been used which might hinder the loading efficiency. Therefore, in designing the new complexes we have replaced the bulkier PPh_3 by less steric dimethylphenylphosphine ($PPhMe_2$).

(Scheme 1). Herein, we discuss the synthesis, characterization and photo luminescent studies of the brominated bpy ruthenium (II) complexes.

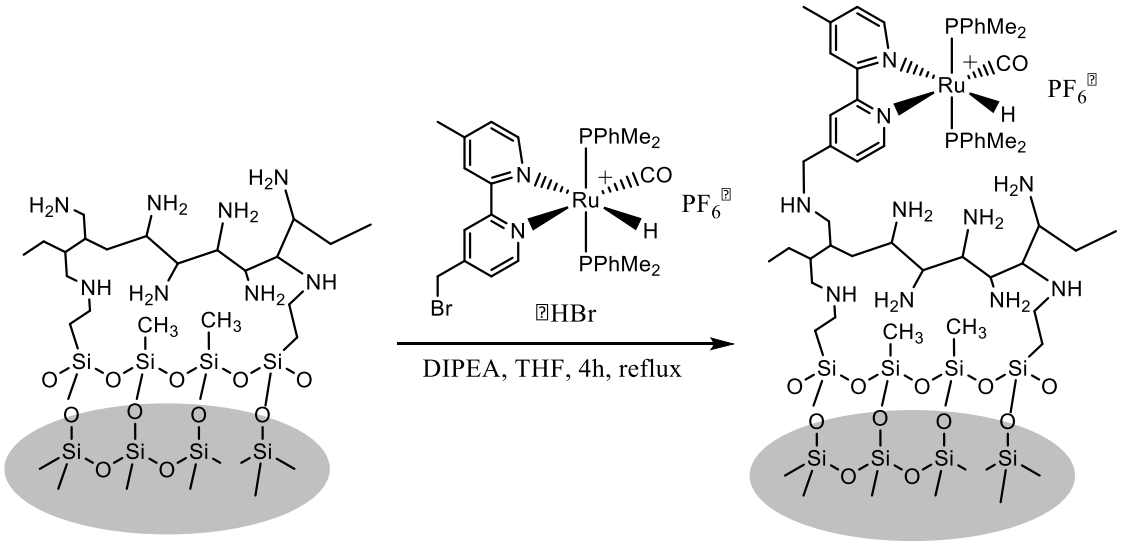

Scheme 1. Coupling of Ru(II) complexes with silica polyamine composites

Experimental

2.1 Materials

Reactions were carried out using standard Schlenk line technique under nitrogen unless otherwise mentioned. Column chromatography was performed using 60 Å pore size 230–400 mesh silica gel (Sorbent Technologies) and 58 Å pore size activated neutral alumina (Sigma–Aldrich). All solvents such as ethylene glycol, dichloromethane and hexane used were of reagent grade. Tetrahydrofuran (THF) was distilled from a mixture of sodium and benzophenone. Acetone and ethylene glycol were purchased from Fischer Scientific and VWR International, respectively. Ruthenium dodecacarbonyl, triphenylphosphine and dimethylphenylphosphine (Strem Chemicals) 2,2′–bipyridine, 4,4′–dimethyl–2,2′–bipyridine 2–phenylpyridine, 2–(p–tolyl)pyridine (Sigma–Aldrich) were used without further purifications. Silica Polyamine composite, BP–1 (150 μM–250 μM) was synthesized by previously reported methods using a 7:5:1 mixture of methyltrichlorosilane and 3–chloropropyltrichlorosilane for the silanization step [32]. Silica gel (26.7 nm average pore diameter, 2.82 mL/g pore volume, 84.7% porosity, 422 m^2/g surface area) was obtained from INEOS enterprises Ltd., UK, and was sieved to 150 – 250 μm. DIPEA (N,N–Diisopropylethylamine) was purchased from MP Biomedical LLC and Rhodamine–B needed for measurement of quantum yield was purchased from Sigma −Aldrich. Starting Complexes $K^+[Ru(CO)_3(TFA)_3]^-$and $Ru[(CO)_2(TFA)_2(PPh_3)_2]$ were synthesized according to literature procedure[28,34].

2.2 Methods

2.2.1 Spectroscopic Measurements

^{1}H (δ, TMS), ^{19}F (δ, $CFCl_3$) and ^{31}P (δ, H_3PO_4) solution NMR were performed on a Bruker NMR systems spectrometer at 400 MHz, 376.55 MHz and 162 MHz for proton, fluorine and phosphorus, respectively. IR spectra were taken by using a Nicolet iS7 and Thermo–Nicolet 633 FT–IR spectrometer as KBr pellets. Luminescence data such as steady–state UV–visible absorption and emission spectra were collected on Molecular Devices Spectra Max M2.

2.2.2 Metal Analysis

For the metal analysis, an atomic absorption spectrometric method, using an S Series Thermo Electron Corporation AA Spectrometer was used. The process involved the loading of ruthenium complex on the surface of silica particles (BP–1) followed by its digestion. Digestion was performed by calcining 40 mg of metal loaded silica particles in an oven overnight at 500°C. After the cooling down of particles, these were transferred to a polypropylene tube, combined with 0.5 mL of concentrated hydrofluoric acid and then with 0.5 mL of modified aqua regia (made by mixing concentrated nitric acid with concentrated hydrochloric acid in 1:6 ratios) and final volume was made 4.5 mL by diluting with DI water [35]. All the particles were dissolved and made translucent by vortexing the sample solution for few seconds. Spectrometric data were collected by running standard solutions of ruthenium complex ranging from 5–90 ppm followed by sample which gave the linear relationship. After then, we calculated the loading of ruthenium on the composite surface which was 0.075 mmol on per gram of BP–1.

2.2.3 Excited–State Lifetime Measurements

Time-resolved luminescence decay measurements were performed by time correlated single photon counting (TCSPC), using the Quantum Northwest FLASC 1000 sample Chamber (Spokane, WA). Pulsed excitation at 470 nm and a repetition rate of 50 KHz (external trigger) from a LDH–P–C 470 laser diode (PicoQuant, Berlin, Germany) were used to excite the complex for time dependent studies. The luminescence decays were collected in the FLASC 1000 orthogonal to the excitation beam path and magic angle polarization condition [36 −38] using a 620/50 nm bandpass filter (Chroma, Rockingham, VT, USA) to isolate the emissions and excitation scatter. All the measurements were taken at room temperature under normal atmospheric pressure. The decay curves were collected using the NanoHarp 250 PCI board (PicoQuant, Berlin) with a timing resolution of 560 ps/channel until 4×10^4 counts were reached. For the measurement of luminescent lifetime FluoFit Pro V4.2.1 (PicoQuant, Berlin) analysis software package [39] was used and reported as the intensity average based on a multiexponential model. The magic–angle intensity decay is given by formula:

$$I(t) = \sum_{i=1}^{n} A_i \, e^{-t/\tau_i} \qquad (1)$$

In this model, τ_i is the excited state lifetime and A_i is the amplitude of the i^{th} component. The intensity average lifetime is given by:

$$\langle\tau\rangle = \frac{\sum A_i\tau_i^2}{\sum A_i\tau_i} \qquad (2)$$

The estimated error in average was calculated from the upper and lower 95% confidence limits of the individual decay components, which were determined by the support–plane method [40]. A representative decay curve and goodness to fit are shown Figure 4.

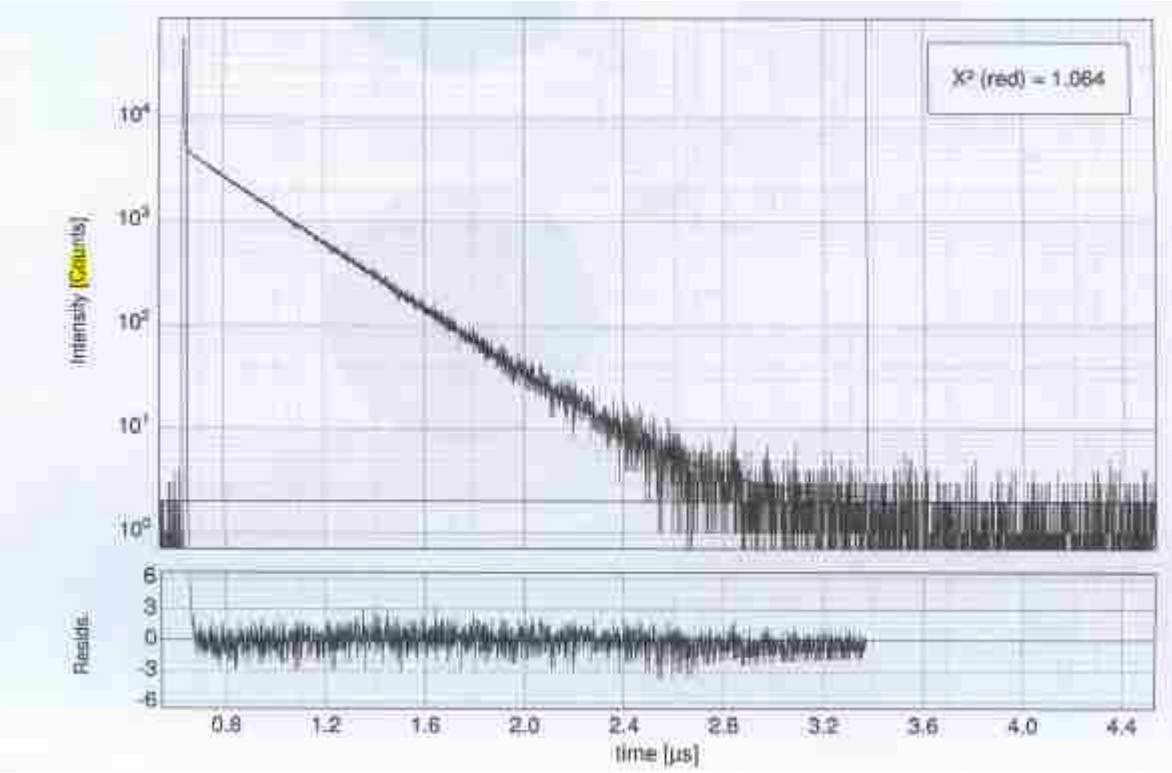

Fig. 4 Lifetime decay curve for 3c with a fitted average lifetime of 0.27µs.

2.2.4. Solid State Structure of complexes

X–ray diffraction data for all **1a**, **1b**, **2** and **3a** were collected at 100 K on a Bruker D8 Venture diffractometer using graphite–monochromated MoKα–radiation (λ–0.71073 Å) radiation. Data have been corrected for absorption using SADABS [41] area detector absorption correction program. Using Olex2 [42], the structure was solved with ShelxT structure solution program using direct method and refined with the ShelXL refinement package using least squares minimization. All non–hydrogen atoms were refined with anisotropic thermal

parameters. Hydrogen atoms were placed in calculated positions using a ridged group model with isotropic thermal parameters U(H) = 1.2Ueq (C) for all C(H,H,H) groups. Calculations and refinement of structures were carried out using APEX [43] SHELXTL [44] and Olex2 software.

2.2.5. Electrochemical Properties

For the measurement of electrochemical properties, a BAS−100 electrochemical analyzer was used. Redox behavior of complexes was studied by using a three electrode standard cell where a glassy carbon was used (diameter 0.1 cm sealed in epoxy resin) as working electrode. Ag/AgCl as a reference electrode and platinum wire was used as auxiliary electrode. During the measurement, the system was deoxygenated by using argon where the metal complexes (1×10^{-3} M) were dissolved in CH_2Cl_2 solution containing 0.1 M [$NBu_4^+PF_6^-$] as supporting electrolyte.

Synthesis

The starting ionic complex $K^+[Ru(CF_3COO)_3(CO)_3]^-$ and phosphine complex $Ru[(PPh_3)_2(CO)_2(TFA)_2]$ were synthesized according to a published procedure [28,34]. Spectroscopic data of all new compounds are summarized in **Table 1**. For **1a** and **3c** result of elemental analysis is also provided.

3.1 Synthesis of $Ru[(PPh_3)_2(CO)(TFA)(ppy–R)]$(1a)(1b)

For the synthesis of phosphine complexes (**1a**) and (**1b**), $Ru[(PPh_3)_2(CO)_2(TFA)_2]$, (**B**) (100 mg, 0.109 mmol), was treated with 2–phenylpyridine (18.46 mg, 0.119 mmol) or 2–(p–tolyl)pyridine (20.19 mg, 0.119 mmol) in ethylene glycol (15 mL) and stirred for 72 h at 140 °C under nitrogen atmosphere. When the color of the reaction mixture turned to green–yellowish, the reaction was cooled to room temperature and then filtered and washed three times with DI water to remove ethylene glycol. The solid was collected by centrifugation at 3000 rpm, washed 2× in DI water, followed by centrifugation, and then washed 1× with diethyl ether. Following the ether wash and rotary evaporation, the product was dissolved in a small amount of methylene chloride and then purified by neutral alumina column in a 1:1 mixture of hexane and methylene chloride as eluent. Out of two bands, the slower green–yellowish band was collected and solvent was removed using a rotary evaporator followed by drying under high vacuum overnight. It gave the green–yellowish powder of $Ru[(PPh_3)_2(CO)(TFA)(ppy)]$ (**1a**) (30mg, 29.57%) and $Ru[(PPh_3)_2(CO)(TFA)(ppy–Me)]$ (**1b**) (35mg, 33.98%) respectively. **1a. Elemental Analysis 1a.** Calculated: 65.21%, 4.16%, N −1.52%, P −6.73%, found: C–67.38%, H–4.49%, N–1.80%, P–7.32%. **IR in KBr**: 3047 cm^{-1} (w) 1931 cm^{-1} (vs), 1684 cm^{-1} (vs), 1433 cm^{-1} (m)**,** 695 cm^{-1} (vs)**,** 521 cm^{-1} (vs) **^{1}H NMR in CD_2Cl_2** (400 MHz, δ, relative to TMS): 6.73–8.78 (m, 38H) **^{19}F NMR** δ= −75.39 (s), **^{31}P NMR** δ = 33.50 (s) **1b IR in KBr:** 2900–3100 cm^{-1}(w). 1931 cm^{-1}

(vs), 1685 cm $^{-1}$(vs). **^{1}H NMR in CD_2Cl_2** (400 MHz, δ, relative to TMS): **1b** 6.56–8.78 (m, 37H), 1.93 (s, 3H). **^{19}F NMR** δ= −75.27 (s), **^{31}P NMR** δ= 34.10 (s).

3.2 Synthesis of $Ru[(PPhMe_2)_2(CO)_2(TFA)_2]$ (2)

The ionic complex $K^+[Ru(CO)_3(TFA)_3]^-$ (300 mg, 0.54 mmol) was refluxed with dimethyl phenyl phosphine (150 mg 1.08 mmol) in acetone solution for 24 h under a nitrogen atmosphere. The reaction was monitored by thin layer chromatography (TLC) periodically. After reaction the solvent was removed by rotary evaporation and the residue was dissolved in methylene chloride and chromatographed on a silica gel column. Elution with DCM/acetone solution (98:2 v/v) gave two colorless bands. The faster moving band was collected and solvent was removed by using rotary evaporation and then dried for overnight under high–vacuum. The product was obtained (80 mg; 27%) as a shiny milky powder **2**. **IR in KBr** 1200 cm $^{-1}$ (vs), 1685 cm $^{-1}$(vs), 2000 cm $^{-1}$(vs), 2062 cm $^{-1}$(vs), 2800 cm $^{-1}$–2950 cm $^{-1}$(w). **^{1}H NMR** (400 MHz, $CHCl_3$, δ, relative to TMS): 7.47−7.52 (2s, 10H), 1.83 (s, 12H), **^{19}F NMR** δ= −74.16 ppm (s), **^{31}P{^{1}H} NMR** δ= 4.8 (s)

3.3 Synthesis of $Ru[(PPhMe_2)_2(CO)(H)(bpy–R)]^+[PF_6]^-$ (3a), (3b) and (3c).

Reaction of complex **2** (100 mg, 0.15 mmol) with 2,2′–bipyridyl (25 mg, 0.15 mmol) in ethylene glycol (20 mL) at 140 °C for 72 h produced an orange colored solution of the cationic complexes of **3a** while the same reaction heated under the same condition for 84 h with 2,2′–bipyridyl and 4,4′–dimethyl 2,2′–bipyridyl (28 mg, 0.15 mmol) gave reddish–yellow solution of **3b** and **3c** respectively. Both solutions were treated with an aqueous solution of NH_4PF_6 (concentration 1gm/10 mL) drop wise until a precipitate was observed (6.5 mL). The resulting solution was refrigerated overnight to promote the complete precipitation, filtered and the residue was washed several times with DI water to remove ethylene glycol, followed by centrifugation and finally washed with diethyl ether. The resulting product was dissolved on

5:2:2 hexene/MeOH/CH_2Cl_2 and then chromatographed using neutral alumina using the same solvent mixture as eluent which gave a single product band. Complete removal of solvent followed by drying under high vacuum for overnight gave Ru[$(PPhMe_2)_2$(CO)(TFA)(2,2′–bipyridyl)]$^+$[PF_6]$^-$ (40 mg, 28.23%), (**3a**), [Ru$(PPhMe_2)_2$(CO)(2,2′–bipyridyl)(H)]$^+$[PF_6]$^-$ (42mg, 33.68%), (**3b**) and [Ru$(PPhMe_2)_2$(CO)(4,4–dimethyl–2,2′–bipyridyl)(H)]$^+$[PF_6]$^-$ (38 mg, 29.47%), **3c**. The complex **3a** has TFA while **3b** and **3c** have hydride coordinated to the central metal ion. (**3a**) **IR in KBr** 3055 cm^{-1}–2850 cm^{-1} (w), 1921 cm^{-1} (vs), 1616 cm^{-1} (s) 840 cm^{-1}(vs). **^{1}H NMR** (400 MHz, $CHCl_3$, δ, relative to TMS): 6.66–8.51 (m, 18H), 1.57 (s, 12H), **^{19}F NMR** (2s, −71.78, −73.80), **^{31}P{^{1}H} NMR** (s 3.37)(−134 to −155 (5s) (**3b**)**. IR in KBr** 2850 cm^{-1}–2964 cm^{-1}(w) 2028 cm^{-1}(w), 1961 cm^{-1}(vs), 838 cm^{-1} (vs). **^{1}H NMR** (400 MHz, $CHCl_3$, δ, relative to TMS): 6.66–8.23 (m, 18H), (s, 12H), −12.36(t, 1H, ^{3}J=20) **^{19}F NMR** (2s, −72.09, −73.98), **^{31}P{^{1}H} NMR** (s, 7.72), −134 to −155(5s) (**3c**) **Elemental Analysis (**calculated: C–47.35%, H–4.80%, N–3.81%, P–12.63%, found: C −46.58%, H −4.82%, N −3.65%, P − 13.5%) **IR in KBr** 2875 cm^{-1} (w), 2077 cm −1 (w), 1970 cm^{-1} (vs), 908 cm^{-1} (vs), 841 cm^{-1} (vs), **^{1}H NMR** (400 MHz, $CHCl_3$, δ, relative to TMS): 6.72–8.75 (m, 16H), 2.48–2.51 (2s, 6H), 1.52–1.55 (m, 6H), 1.48–1.51 (m, 6H), −12.5 (t, 1H, ^{3}J =20), **^{19}F NMR** (2s, −73.95, −71.98) **, ^{31}P{^{1}H} NMR** 8.23 (S), 3.36(s), −135 to −153 (5s)

3.4 Synthesis of [RuPPh$Me_2)_2$(CO)(H)(4–bromomethyl,4′–methyl–2,2′–bipyridine]$^+$[PF_6]$^-$ (3d and 3d′)

Chelating monobrominated diimine ligand, [4–(bromomethyl)–4′–methyl–2,2′–bipyridine], (bpyBr) was synthesized according to previously published procedure [45]. The reaction of complex **2** (100 mg, 0.15 mmol) with [4–(bromomethyl),4′–methyl–2,2′–bipyridine] (39.30 mg, 0.15 mmol) in 15 mL of deoxygenated ethylene glycol for 84 h at 140°C gave the deep red color of **3d** and **3d′**. Resulting reaction mixture was treated with aqueous solution of

NH_4PF_6 (1 g/10 mL) drop wise until it gave precipitates. The resulting ionic solution was kept under refrigerator for overnight to promote the complete precipitation, filtered and residue was washed several times with DI water to remove ethylene glycol, followed by centrifugation and finally washed with diethyl ether. After complete removal of ethylene glycol, the product was dissolved on 5:2:2 hexane/MeOH/CH_2Cl_2 and then chromatographed using neutral alumina using the same solvent mixture as eluent which gave the single product band. Complete removal of solvent followed by drying under high vacuum for overnight gave yellow–reddish powder of **3d** and **3d′**. (35 mg yield 24.84%). **IR in KBr** 2870 cm^{-1} (w), 2075 cm^{-1}(w)1970 cm^{-1} (vs), 908 cm^{-1}(vs), 841 cm^{-1} (vs), 557 cm^{-1} (vs). **^{1}H NMR** (400 MHz, $CHCl_3$, δ, relative to TMS: 6.6–9.1 (m, 15H), 4.61–4.91 (m, 2H), 1.41–2.65 (m, 15H), −12.45 (triplet of triplet, 1H), **^{19}F NMR** δ= −71.48 (s) −75.54(s) **^{31}P{^{1}H} NMR** δ= 1.63 (s), 3.02 (s) , −153 to −135 (5s)

3.5 Genera procedure for coupling of complex with silica particles

BP–1 microparticles (1.0 gm;150–250 μM) was added and degassed on the freshly prepared THF solution followed by 200 mg (0.245 mmol) of brominated ruthenium complex (**3d–3d′**) and 0.246 mmol DIPEA (N,N–diisopropylethylamine). The reaction was refluxed for 4 h under nitrogen atmosphere, stirred from the top and periodically monitored by TLC. When all the metal complex and DIPEA was consumed, reaction was stopped and all the solvent was removed and washed with methanol for three times. Metal loaded silica particles were then dried under high vacuum line and characterized by means of IR spectroscopy where it showed the characteristic peak of metal carbonyl group (1968 cm^{-1}).

Results and Discussion

4.1 Compound synthesis and reaction pathways

A series of reactions shown in Schemes 3.1–3.6 depict the synthetic pathways for all the luminescent complexes of this series. The starting material (**A**) and (**B**) needed for the synthesis of **1a** and **1b** were synthesized according to already published procedure, [28, 35] while the other complexes were synthesized some modified pathways. The synthetic processes involve the carbonyl and TFA (CF_3COO^-) groups' replacements, which were monitored by IR and ^{31}P NMR spectroscopy.

The first sets of cyclometallated complexes with 2–phenylpyridine, (**1a**) and 2–(p–tolyl) pyridine, (**1b**), with general formula $[Ru(PPh_3)_2(CO)(TFA)(ppy–R)]$, were synthesized from the phosphine complex as shown in Scheme 1.

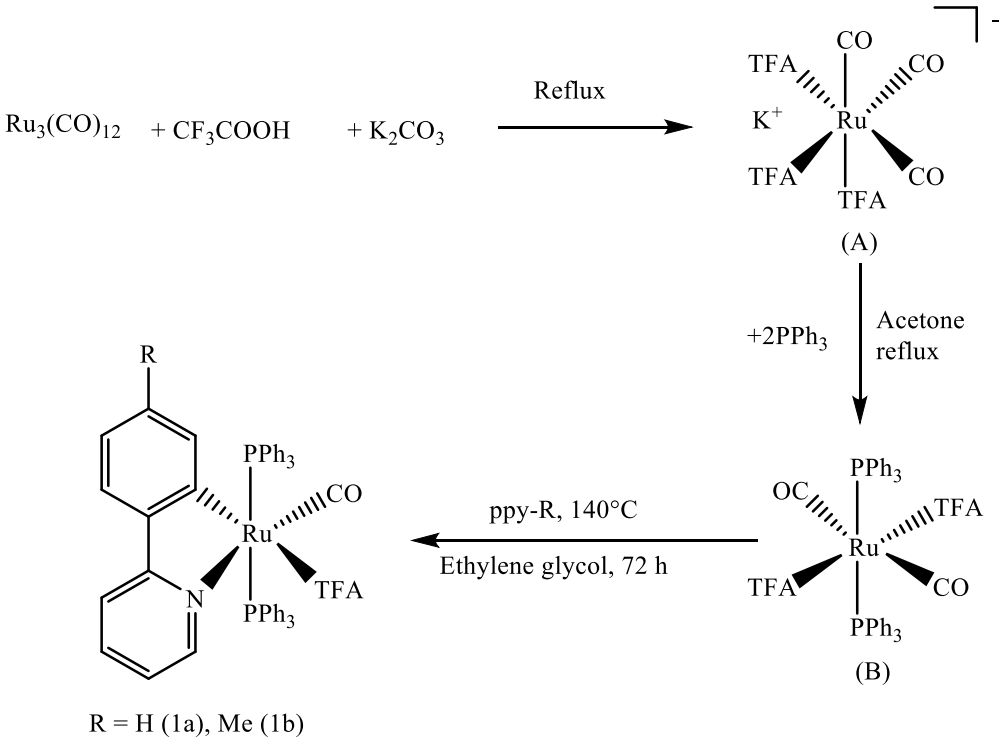

Scheme 2. Synthesis of complexes **1a** and **1b**

The reaction of (**B**) with 2–phenylpyridine and 2–(p–tolyl)pyridine at 140°C for 72 h in ethylene glycol gave the crude product of complex (**1a**) and (**1b**) respectively. After purification by column chromatography (using 1:1 mixture of DCM:Hexane), both of these complexes were characterized by IR, ^{1}H NMR, $^{31}P–\{1H\}$ NMR, ^{19}F NMR and UV–Vis spectroscopy. The structure was further characterized by single X–ray diffraction analysis.

The phosphine complex with formula $[Ru(PPhMe_2)_2(CO)_2(TFA)_2]$, (**2)** was prepared from the starting material (**A**) by refluxing with dimethyl phenyl phosphine in acetone for 12 h as shown below (scheme 3).

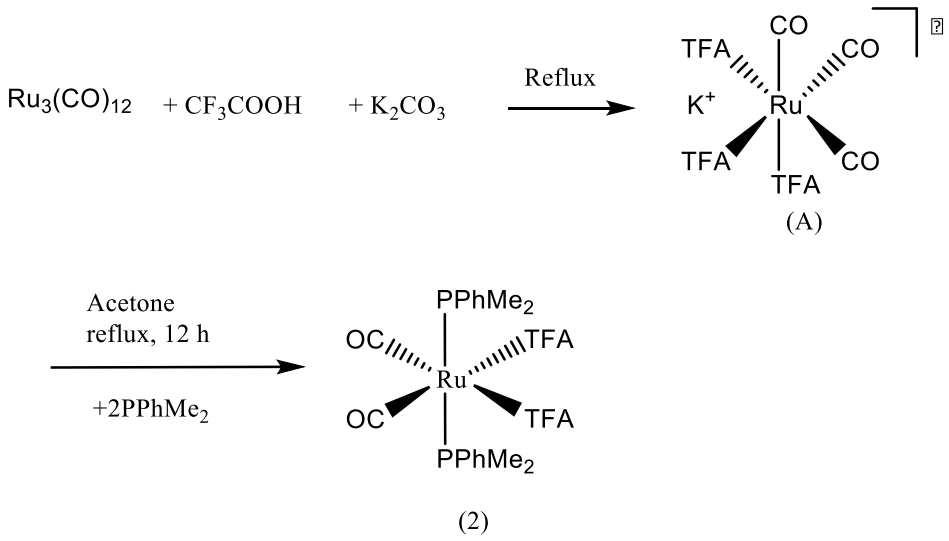

Scheme 3. Synthesis of complex (**2**)

The complex was purified by using alumina column with CH_2Cl_2/acetone (97:3 and characterized by infrared, ^{1}H NMR, $^{31}P–\{^{1}H\}$ NMR and ^{19}F NMR. The structure was further characterized by single X–ray diffraction analysis.

The second of sets of luminescent ruthenium complexes with general formula $[Ru(PPhMe_2)_2(CO)(L)(bpy–R)][PF_6]$, (**3a, R=H, L=TFA)**, (**3b, R=H, L=H)** and (**3c, R=Me,**

L=H) were prepared according to the Scheme 4.3. Reaction of (**2**) with 2,2′–bipyridyl ligand at 140°C for 72 h in ethylene glycol gave cationic complex $[Ru(PPhMe_2)_2(CO)(TFA)(2,2'–bipyridyl)]^+$ which was precipitated by using aqueous solution of NH_4PF_6 to get complex (**3a).** The reaction of same metal complex with diimine chelating ligands 2, 2′ −bipyridyl and 4,4′–dimethyl–2,2′–bipyridyl gave the hydride complexes with formula $[Ru(PPhMe_2)_2(CO)(H)(2,2'–bipyridyl)]^+$ and $[Ru(PPhMe_2)_2(CO)(H)(4,4'–dimethyl–2,2'–bipyridyl)]^+$ when heated up to 84 h respectively. Both of these were precipitated by using the aqueous solution of NH_4PF_6 to get **(3b)** and **(3c)** respectively.

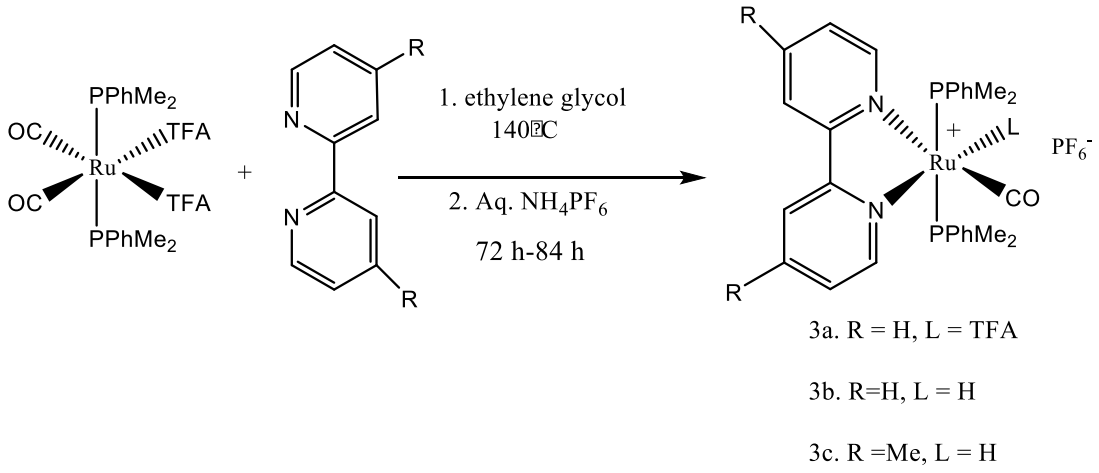

Scheme 4. Synthesis of complexes **3a**, **3b** and **3c**

All three complexes were purified by using an alumina column in a 5:2:2 mixtures of hexane, methylene chloride and methanol respectively and characterized by infrared, ^1H NMR, $^{31}P–\{^1H\}$ NMR and ^{19}F NMR and UV–Vis spectroscopy. The structure of complex **3a** was further characterized by single crystal X–ray diffraction analysis.

For the synthesis of complex (**3d** and **3d′**), 4, 4′–dimethyl–2, 2′–bipyridyl ligand was brominated to get the [4–(bromomethyl),4′–methyl–2, 2′–bipyridine] by following the procedure from already published literature **[**45]. The reaction of compound (**2**) with brominated ligand in ethylene glycol at 140°C for 84 h followed by precipitation using aqueous solution of NH_4PF_6 gave the isomeric mixture of complex (**3d**) and (**3d′**) (Scheme 4).

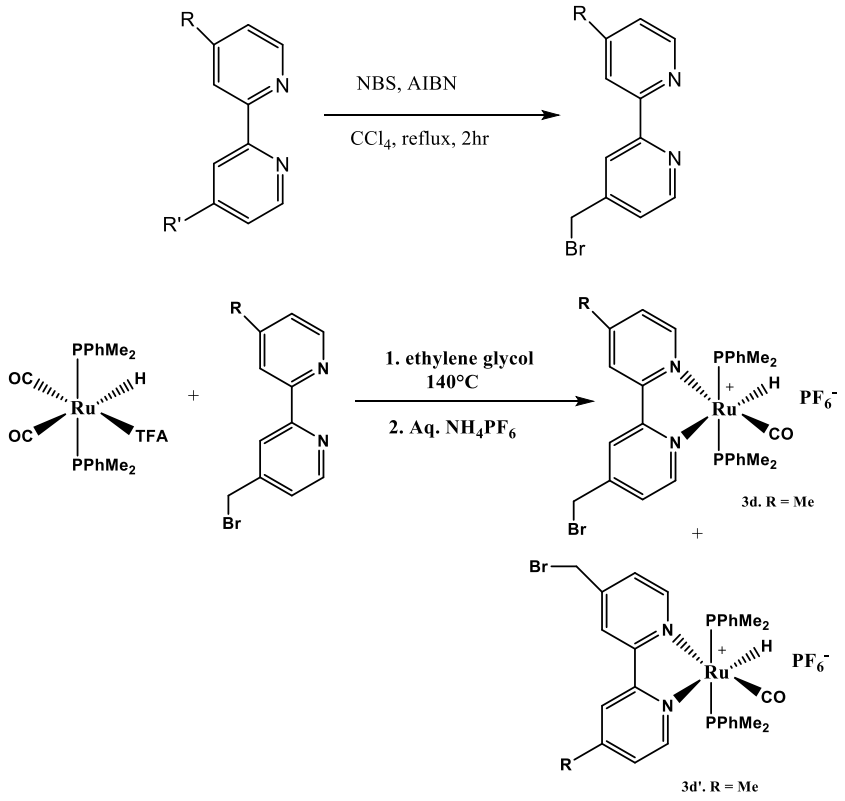

Scheme 5. Synthesis of brominated complexes **3d** and **3d′**

The complex was purified on an alumina column by using 5:2:2 mixtures of hexane, methylene chloride and methanol respectively and characterized by infrared, ^{1}H NMR, $^{31}P-\{^{1}H\}$ NMR, ^{19}F NMR and UV–Vis spectroscopy.

The diimine complexes **3b**, **3c**, **3d** and **3d′** were changed to the hydride complexes with the replacement of TFA by hydride ion on heating the reaction mixture more than 72 h – 84 h.

The hydride group directly coordinates to the metal center by means of β–elimination reaction where there is the direct participation of solvent. The reaction is supposed to proceed with the following mechanism.

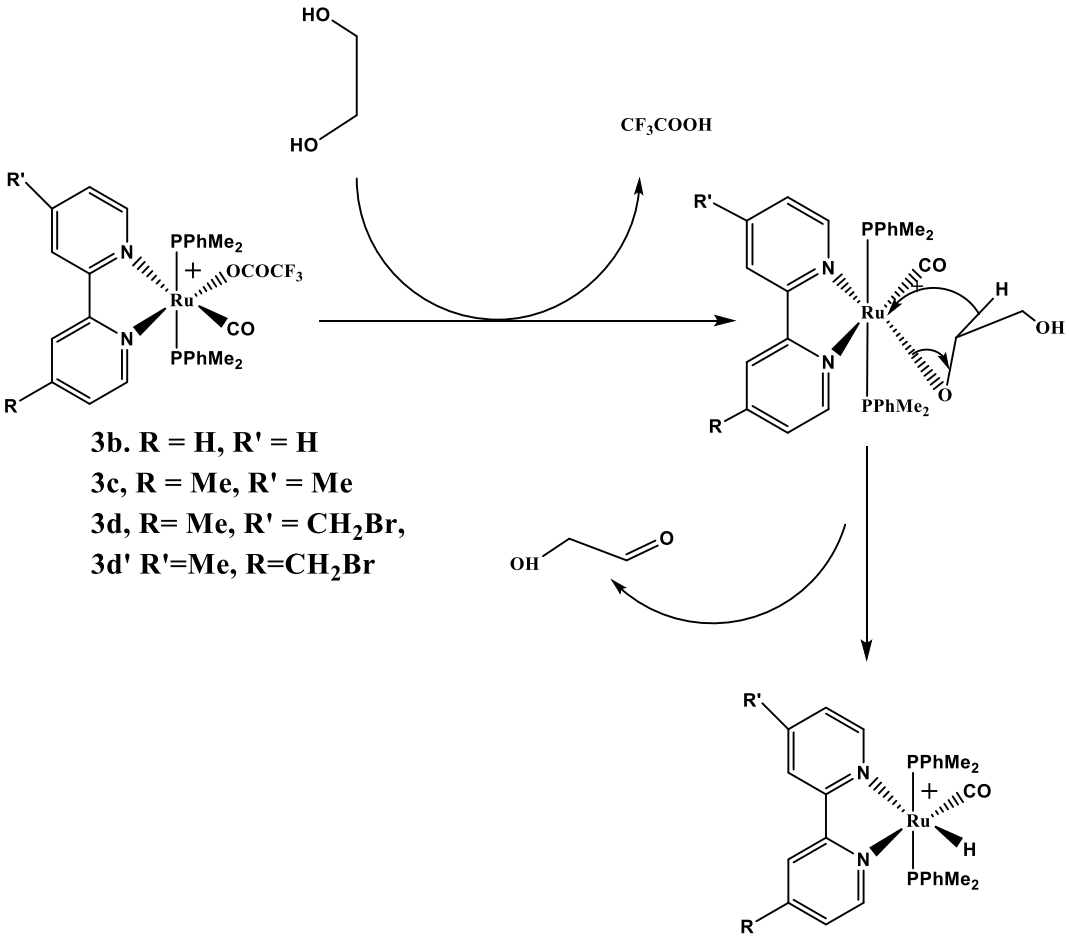

Scheme 6. Proposed mechanism for β −elimination reaction

The brominated complexes **3d** and **3d′** were loaded on the surface of silica polyamine composites, BP–1 by refluxing with tetrahydrofuran (THF) for four hours in the presence of diisopropylamine (DIPEA) as shown in Scheme.

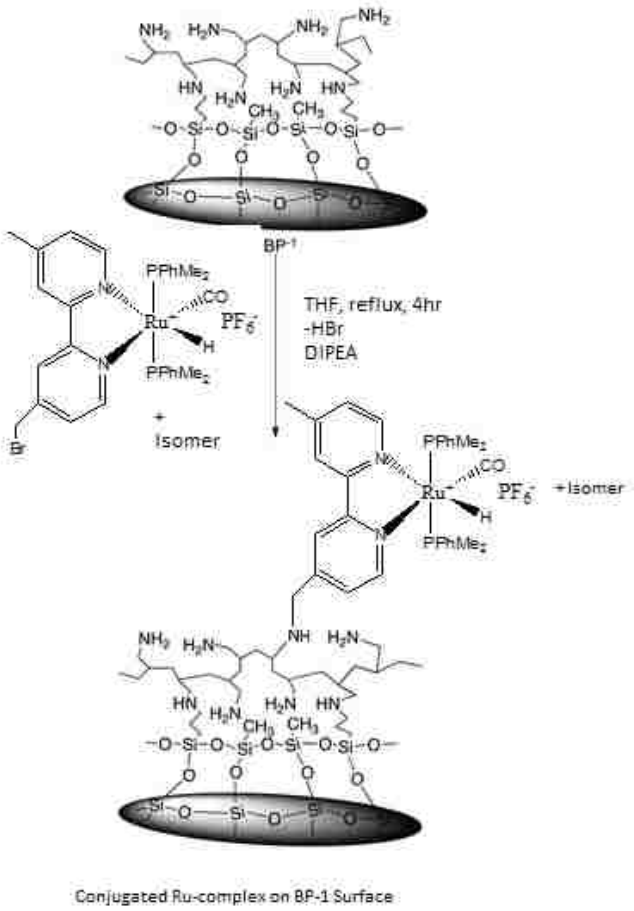

Scheme7. Loading of **3d** and **3d′** on BP–1 surface

4.2. Spectroscopic Characterization

4.2.1 Infrared Spectral Characterization

Infrared spectroscopic data of the newly synthesized complexes provided valuable information about their structures. The IR stretching frequency of the carbonyl group serves as a reliable tool for structural comparison with starting materials. Since π*–orbital on the M–CO bond has higher tendency to accept electrons from central metal ion, carbon–oxygen (CO) bond order is reduced after the coordination of electron–rich ligands with central metal ion. Therefore, the electronic environment around the central metal is manifested on the ν(CO) stretching frequency of the complexes. If there are more electron donor ligands coordinated, IR absorption frequency moves toward lower energy because back bonding ability of metal significantly increases.

In the cyclometallated complexes with chelating ppy–R ligand, ν(CO) stretching frequencies for **1a** and **1b** appear at 1938 and 1931 cm^{-1} respectively while the IR stretching values for the starting complex (**B**) appears at 2066 and 2002 cm^{-1}. This clearly indicates the presence of only one carbonyl group on the new complexes and electron rich environment on both **1a** and **1b** compared to starting complex (**B**). There is a small reduction in the ν(CO) stretching value of **1b** relative to **1a** which is caused by the electron donating methyl group on the 4–position of phenyl ring. The ν(C–H) stretching frequency for this group appears between 2800−2900 cm^{-1}. Both of those complexes have one electron withdrawing CF_3COO^- group (TFA), which has characteristic IR stretching peak at 1685 cm^{-1} caused by C=O stretching.

In octahedral complex **2,** two carbonyl and two CF_3COO^- groups are coordinated to the central metal ion. Since there are two electron donor dimethylphenylphosphine groups on this complex, two M–CO stretching bands appear at 2000 cm^{-1} and 2062 cm^{-1}, at a lower energy

region compared to the starting material **A**. That there are two values of υ(CO) clearly indicates the coordination of two carbonyl groups with central metal atom. The broad peak that appears at 1685 cm^{-1} is assigned to the two M–OC(O)CF_3 stretching band. Electron rich environment of new complexes is also manifested on the lower stretching frequencies carbonyl bond of CF_3COO^- groups.

Ionic complex **3a** has CF_3COO^- group which shows its characteristic stretching band at 1680 cm^{-1} while **3b, 3c, 3d** and **3d′** have Ru–H bond at that position and is supported by the observation of stretching frequency in the region ranging from 2000–2100 cm^{-1} recorded by FT–IR [33]. Out of four these complexes, M–CO bond stretches around 1970 cm^{-1} for **3a** and 1961 cm^{-1} for **3b** while others stretch between 1931 cm^{-1} – 1935 cm^{-1}. The little lower value of the ν(CO) stretching frequency of **3b** is caused by highly electron donating hydride group coordinated to the central metal. In the case of complexes, **3c, 3d** and **3d′** there is the combined effect of hydride ligand and methyl groups on 4, 4′–position of bipyridyl group to lower the ν(CO) stretching frequency. All these complexes show sp^3 hybridized C–H bonds stretch between 2850 cm^{-1} – 2950 cm^{-1}. Furthermore the introduction of diimine ligands makes the rich electronic environment surrounding the central metal whose stretching band appears from 800 – 840 cm^{-1}. IR lines between 550 cm^{-1} – 560 cm^{-1} has been assigned for asymmetric stretching mode of PF_6^- group [46].

A good comparison can be made between hydride ruthenium complexes having triphenylphosphine groups with dimethylphenylphosphine in terms of their ν(CO) stretching frequencies. Since triphenylphosphine is good sigma donor and good π–acceptor, back donation from metal $d_\pi \rightarrow L_{\pi^*}$orbital occurs easily resulting the lower electron density on metal–carbonyl bond. Hence it has higher ν(CO) value. On the other hand, dimethylphenylphosphine is a good

σ–donor but a very weak π–acceptor and reduces the M_{π}–back donation. It increases the electron density on M–CO bond and thus converts the triply bonded carbon–oxygen to a double bonded one [47, 48].

Table 1. IR and NMR Data

compound	**IR in KBr (ν_{co},cm^{-1})[a]**	**^{1}H (TMS) NMR (δ, ppm)[b]**	**^{31}P (H_3PO_4) NMR (δ, ppm)[b]**	**^{19}F ($CFCl_3$) NMR (δ, ppm)[b]**
1a	1685, 1939	7.1–8.5 (38H)	34.04 (s, 2P)	−75.12 (s, 3F)
1b	1685, 1931, 2900–3100	1.55(3H), 6.28–8.51 (37H)	33.98 (s, 2P)	−75.39 (s, 3F)
2	1685, 2000, 2062	2.2 (12H), 7.4–7.8 (10H)	4.35 (s, 2P)	−74 (s, 6F)
3a	1970, 1680	1.56 (s,12H), 6.68–8.49 (m, 18H)	7.24 (s, 2P)	103 (s, 3F), −73.2 (s), −72.4 (s)
3b	1961,	−12.37(t, 1H), 1.53 (s, 12H), 6.71–8.49 (m, 18H)	7.22 (s, 2P), −140 (m, 1P)	−73.95 (s), −72.9 (s)
3c	1931	−12.47 (t 1H), 1.52 (s, 12H), 2.5 (s, 6H), 6.75–8.27 (m, 16H)	7.91 (s, 2P) −155 (m, 1P)	−73.95 (s), −71.89 (s) (1F)
3d–3d′	1931	−12.40−12.46 (t, 1H), 1.47 (m, 12H), 2.47 (m, 3H), 4.69 (m,2H), 6.44–9.02 (m,16H)	1.72 (s, 2p), 7.91 (s, 2P) −155 (m,1P)	−73.74 (s), −71.48 (s)

[a]Data were collected on KBr

[b]Data were collected on methylene chloride, chloroform and acetone

4.2.2 NMR Spectral Analysis

^{1}H, ^{19}F and ^{31}P NMR spectra of these complexes taken on chloroform show the consistency of predicted structures of d^6 metal complexes. Except **1a**, all other complexes have both aliphatic and aromatic protons. Aliphatic protons are present in the form of methyl group of cyclometallated complex **1b** and phosphine as well as diimine ligand in rest of the compounds. The methyl protons attached on the dimine ligands have higher chemical shift value than those on the methyl groups on phosphine ligands. The chemical shift values as well as coupling constant of all protons are presented on **Table 1**. In all complexes, chemical shift values for aromatic protons range from δ = 6.0–8.5 where phenyl protons on phosphine groups appear as multiplets. For the brominated complex, two sets of isomers **3d** and **3d′** coexist and their effects are well manifested throughout the whole NMR scale by doubling and overlapping of protons. After bromination, the two SP^3 hybridized protons on CH_2 group are diastereostopic and appear as second order AB patterns around δ= 4.5 with a number of peaks of unequal intensities. The complexes **3b**, **3c**, **3d** and **3d′** have directly coordinated hydride group with central metal ion that appears between δ= −11.5 to −12.5. In the case of **3b** and **3c**, it appears as a triplet. In the isomeric complexes **3d** and **3d′** there is overlap of the triplets and virtual coupling with the phosphines resulting in a complex pattern of resonances of unequal intensities, arising from the chiral nature of **3d** and **3d′**. Formation of triplet or multiplets is resulted by the coupling hydride with two *cis*–located phosphorous nuclei which is the special characteristics of metal hydrides complexes [49].

^{19}F NMR for **1a** and **1b** appears at δ = −75.12 ppm and δ = −75.39 ppm respectively which is due to presence of CF_3COO^- group. Complex **2** has two peaks between δ= −74 to −76 ppm with slightly different intensities although they should be of equal intensities. Ionic complex

3a also has two types of fluorine; first from the CF_3COO^- group and the second from the PF_6^- on the counter anion. However **3b**, **3c**, **3d** and **3d′** have only one type of fluorine that appears as two singlet between δ = −70 to −80.

^{31}P NMR has been useful in the structural determinations of the complexes. Complexes **1a** and **1b** show only singlet those resonances at δ= 33–34 with respect to H_3PO_4. Size is an important factor in determining the chemical shift and number of isomers formed in octahedral complexes. Since triphenylphosphine ligands are bulky, they tend to form *trans*–isomers to minimize steric hindrance. However, as the size of phosphine group decreases (less bulky), *cis*–isomers are also common. As the cone angle increases, there is gradual downfield shift in NMR spectra [50]. Therefore complex **1a** and **1b** have ^{31}P NMR at lower field region relative to the $PPhMe_2$ complexes. The ^{31}P NMR of complex **2** has only a single sharp peak resonating at δ= 4.35 and thereby indicating the *trans*–position of two phosphine ligands.

The ionic complexes **3a**, **3b**, **3c**, **3d** and **3d′** there are two types of phosphorous peaks i.e. from phosphine ligands and from PF_6^- group, a counter anion to the cationic complex. Since two phosphine ligands are *trans*–position to each other, there is no ^{31}P–^{31}P coupling, singlet sharp peak of phosphine appears around δ= 7.91. However owing to their smaller size, *cis*–locating phosphine are also found to some extent and resonate at δ= 3.43. Except **3a**, all other ionic complexes have hydride ligand directly coordinated to the metal center which causes ^{31}P–$\{^1H\}$ coupling with each phosphorous nuclei thereby resulting a triplet that appears between δ= −11.5 to −12.5 [50]. On the other hand, $[PF_6^-]$ exists as septet in ^{31}P NMR after coupling with six fluorine and ranges from δ= −135 to −153 with an integrated relative intensity of 1:2 ratio compared to the resonance of phosphine ligands [33].

4.3 Crystal Structure Analyses

The structure of neutral ruthenium complexes $[Ru(PPh_3)2(CO)(TFA)(ppy)]$ **1a**, $[Ru(PPh_3)_2(CO)(TFA)(ppy–Me)]$ **1b**, $[Ru(PPhMe_2)_2(CO)_2(TFA)_2]$ and ionic complex $[Ru(pphMe_2)_2(CO)(TFA)(bpy)]^+[PF_6]^-$ were elucidated by single–crystal X–ray diffraction analysis. Both complexes **1a** and **1b** were crystallized in the monoclinic system with space group $p2_1/c$, **2** in the triclinic system with space group P−1 while **3a** was crystalized in monoclinic system with space group Pm.

Compounds **1a** and **1b** were grown by slow evaporation of concentrated chloroform solution in a stream of pentane at room temperature. Similarly crystal structure of complex **2** was grown by slow diffusion of pentane into an acetone solution containing the complex. On the other hand for growing the crystal structure of complex **3a**, slow evaporation of diethyl ether under the concentrated solution of chloroform was used inside the refrigerator. These crystals were mounted on glass fibers with polyisobutene oil. Thermal ellipsoid plots with numbering scheme are shown in figures below. The crystallographic data related to structure and refinement for compounds **1a**, **1b**, **2** and **3a** can be found on table 2. Similarly, bond distances and bond angles are found on table 3–6.

The ball and stick drawing of neutral complex **1a** and **1b** are displayed figure 5 and 6 respectively. Ruthenium complexes **1a** and **1b** display distorted octahedral geometry where 2–phenylpyridine and 2–tolylpyridine along with carbonyl and TFA groups occupy the equatorial position and two phosphine ligands are at the axial position of complexes. In general bond distances and bond angle values of central ruthenium ion with different ligands are not same. This established that ruthenium center was not spaced evenly between electron releasing and electron withdrawing groups.

Complexes **1a** and **1b** are structurally similar to each other except the methyl group in fourth position of 2–phenylpyridine in **1b**. In both complexes two phosphorous ligands are located to *trans*–position to each other in order to minimize the steric interactions. In complexes **1a** and **1b** P(1)–Ru–P(2) bond angles are 178.8°(12) and 177.37°(2) (close to 180°) respectively. The bond angle between two triphenylphosphine in structurally similar osmium complex with **1a** is 176.78(6)° [51]. The metal–phosphorous distances between **1a** and **1b** i.e. average bond length between Ru1–P1 and Ru1–P2 for **1a** is 2.392 Å while the corresponding bond length for **1b** is 2.397 Å. Similar trends are found in metal–phosphorous bond distance even in octahedral iridium complex where average bond distance between central metal and phosphorous atom is 2.390Å [52].

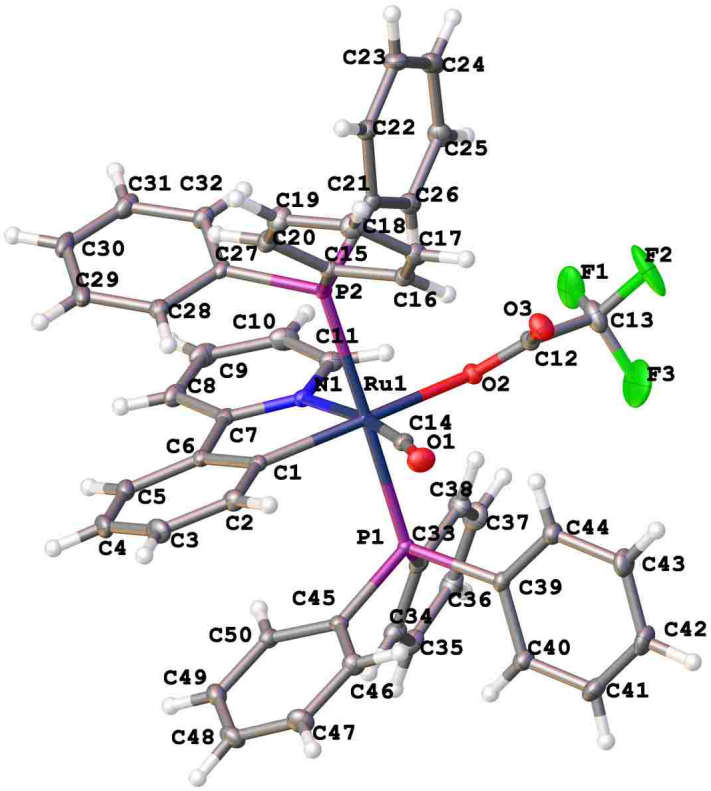

Fig. 5. Solid state structure of Ru[$P(C_6H_5)_3$(CO)(TFA)(ppy)](**1a**) showing the 50% thermal ellipsoids probability level

The Ru(1)–C(1) bond length in complex **1a** and Ru(1)–C(11) in **1b**, are relatively shorter than corresponding Ru −O(CO)CF_3 bond distances. Ru(1)–C(1) bond length in **1a** is 2.152 Å while that for Ru(1)–O(2) is 2.195Å. Similarly Ru(1)–C(11) for **1b** is 2.063 Å while that for Ru(1)–O(2) is 2.201Å. This differential bond distance can be explained in terms of *trans*–effect of coordinating groups. Since the anionic carbon on phenyl group has higher *trans* –effect [53], it not only increases the labiality of TFA group but also lengthens the Ru−TFA bond distance. On the other hand, The Ru(1)–N(1) bond on both complexes are longer than corresponding Ru–CO bond distances. In complex **1a**, Ru(1)–N(1) distance is 2.152 Å and Ru–N(1) in **1b** is 2.153 Å while the Ru(1)–C(14) in **1a** and Ru −C(49) in **1b** are 1.845(13)Å and 1.847(2)Å respectively. In both complexes CF_3COO^- and CO groups are in *cis* −position to each other with C(14)–Ru(1)–O(2) and C(49)–Ru(1)–(O)2 102 (5)° and 112.12(8)° respectively.

The presence of a methyl group in **1b** increases the electron donating ability of the phenyl carbon to the metal center causing the shortening of Ru(1)–C(11) bond in **1b** relative to Ru(1)–C(1) bond in **1a.** This is a good indication of higher donor ability of 2–(p–tolyl)pyridine in **1b** than that of 2–phenylpyridine in **1a**.

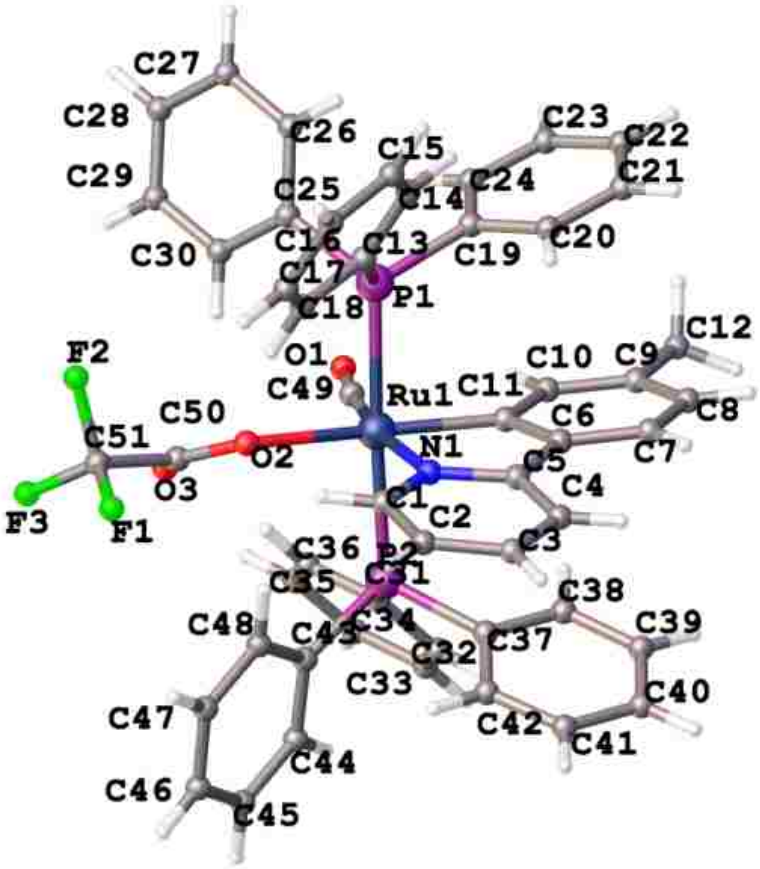

Fig. 6. Solid state structure of Ru[P(C_6H_5)$_3$(CO)(TFA)(ppy–Me)](**1b**) showing the 50% thermal ellipsoids probability level

Important bond length and bond angle data for complex **2** has been given in table 5. Neutral complex **2** also occupies octahedral geometry with two dimethylphenylphosphine ligands in *trans*–position, almost at linear position to each other (180°) with P(1)–Ru–(P)2 bond angle 176.38(5).° Bond length to each phosphine group from central metal ion is almost same via: Ru(1)–P(1) is 2.380(13)Å and Ru(1)–P(2) is 2.379(13). Two carbonyl and two TFA ligands are

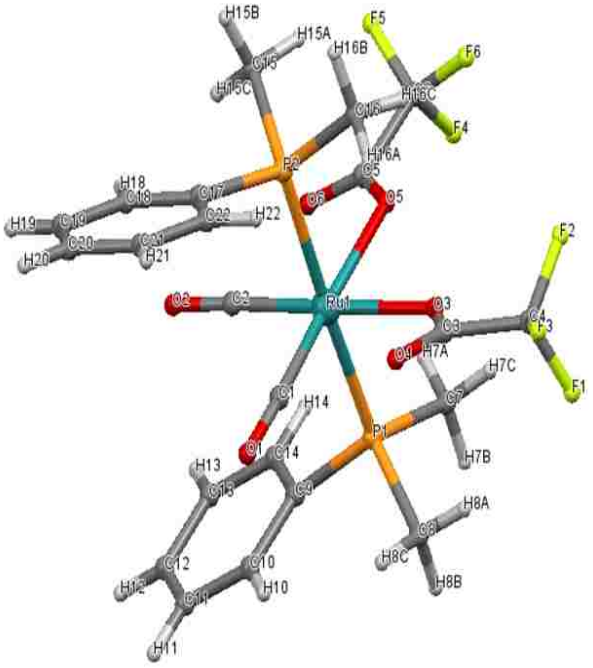

Fig. 7. Solid state structure of $Ru[P(PPhMe_2)_2(CO)_2(TFA)_2]$ (**2**)

located *cis*–position to each other where C(1)–Ru–C(2) bond angle is 87.6(2)° with bond length for Ru(1)–C(1) and Ru(1)–C(2) are 1.864(5) Å and 1.889(5) Å respectively. Similarly each CF_3COO^- groups are 2.101(3) Å farther from central metal ion. Two labile trifluoroacetate (CF_3COO) groups are also located at *cis*–position to each other with bond angle O(3)–Ru–O(5) 79.71(13). As such each Ru–CO bonds are relatively shorter than corresponding Ru–$O(CO)CF_3$ bonds. Possible reason behind this short bond length might be related to their weak σ–donating and stronger π–accepting tendency.

The solid state structure of **3a** is shown in the Fig. 8. The important crystallographic data are given in Table 2 and selected bond length and bond angles in table **6**. The complex **3a** has two monodentate dimethylphenylphosphine groups in *trans*–position to each other. The presence

of anionic $[PF_6]^-$ group assures the positive charge on complex. All ligands in this complex are arranged almost in octahedral geometry around central Ru (II) ion with bite angle 78.61°(15). Two phosphorous atoms of $PPhMe_2$ groups are bound to central metal ion in completely symmetrical fashion i.e. bond length of both Ru–P(1) and Ru–(P)2 is 2.37(12) Å. They are almost in linear position to each other with P(1)–Ru–P(2) angle 175.49(6) Å. The distance between carbonyl carbon and central ruthenium ion is the shortest one [1.86(5) Å] which is similar those observed for octahedral osmium and rhenium complexes [54–56]. It is in the *cis*–position to oxygen atom of TFA group with C(1)–Ru–O(2) bond angle of 96.46(18) Å. The shorter Ru–CO bond length might be resulted by its weaker σ–donor and stronger π–acceptor ability than bipyridyl nitrogen on its *trans*–position. The two nitrogen atoms on 2,2′–bipyridyl ligands are unsymmetrically located around central metal ion with Ru–N(1) and Ru–N(2) bond distance 2.05(4) Å and 2.10(4) Å respectively. The Ru–N bond on *trans*–position to CO group is longer than that of TFA group.

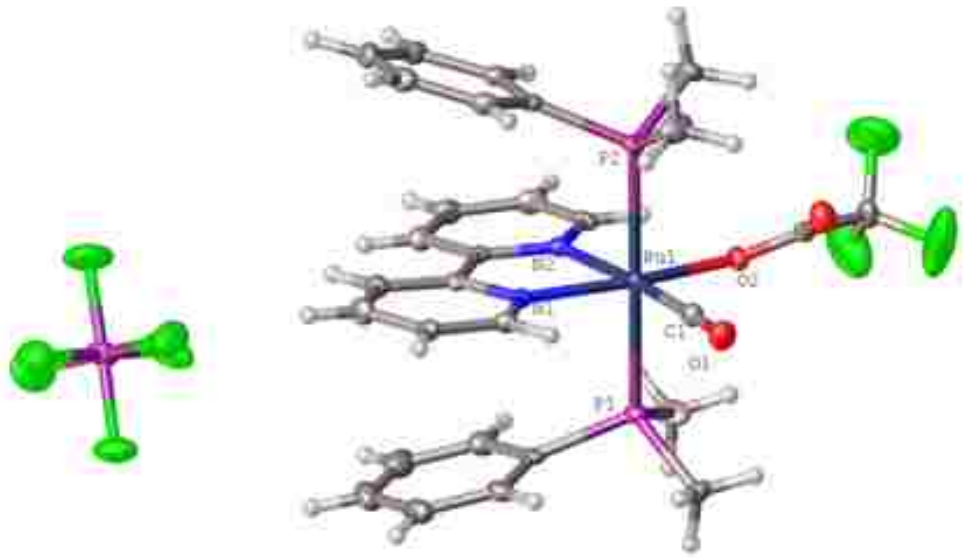

Fig. 8. Solid state structure of $[RuP(PPhMe_2)_2(CO)(TFA)(bpy)][PF_6]$ (**3a**) showing the 50% thermal ellipsoids probability level

Crystal structures of neutral and ionic metal complexes have some special features. Both of them have phosphine and carbonyl ligands. Complexes **1a**, **1b** and **2** are neutral and have the plane of symmetry while ionic complex **3a** has no plane of symmetry.

Table 2. Summary of crystal data and structure refinement for compound **1a**, **1b**, **2** and **3a**

Compound	**1a**	**1b**	**2**	**3a**
Empirical formula	$C_{50}H_{38}F_3NO_3P_2Ru$	$C_{51}H_{40}F_3NO_3P_2Ru$	$C_{22}H_{22}F_6O_6P_2Ru$	$C_{29}H_{30}F_9N_2O_3P_3Ru$
Formula Weight	920.82	934.85	659.40	819.53
Temperature(K)	100	100	100	100
Crystal System	monoclinic	monoclinic	triclinic	monoclinic
Space group	$P2_1/C$	$P2_1/C$	p−1	pn
Unit Cell Dimension				
a/Å	11.5330(7)	11.6934(12)	9.3321(10)	9.3528(6)
b/Å	17.7155(10)	17.5395(18)	10.568 (11)	14.9723(10)
c/Å	20.5179(12)	20.976(2)	15.2421 (15)	12.2752(8)
α/°	90	90	97.779(4)	90
β/°	97.2673(18)	94.796(3)	96.729(4)	111.739
γ/°	90	90	115.380(3)	90
Volume/$Å^3$	4158.4(4)	4287.1(8)	1319.7(2)	1596.68
Z	4	4	2	2
ρ_{calc} g/cm^3	1.471	1.448	1.659	1.705
μ/mm^{-1}	0.313	0.499	0.793	0.729
F(000)	1880.0	1912.0	660.0	824.0
Crystal size/mm^3	0.329×0.228×0.199	0.2×0.05×0.1	0.4×0.4×0.3	0.2×0.15×0.15
Radiation	MoKα (λ = 0.71073)	MoKα (λ = 0.71073)	MoKα(λ= 0.71073)	MoKα (λ = 0.71073)
2θ range for data collection/°	5.816–61.208	5.814–61.256	13.688–52.744	6.51–61.146

Index ranges	$-16\leq h\leq 16, -25\leq k\leq 25, -29\leq 1\leq 29$	$16\leq h\leq 16, -25\leq k\leq 25, -30\leq 1\leq 29$	$11\leq h\leq 11, -13\leq k\leq 13, -19\leq 1\leq 19$	$-13 \leq h \leq 13, -21 \leq k \leq 21, -17 \leq 1 \leq 17$
Reflection collected	**243373**	**141832**	**36012**	**24363**
Independent reflection	**12766[R_{int} = 0.0481, R_{sigma} =0.0185]**	**13166[R_{int}=0.1154 , R_{sigma}=0.0500**	**5293[R_{int}=0.0422, R_{sigma}=0.0254]**	**9732 [R_{int} = 0.0345, R_{sigma} = 0.0501]**
Data/restraint /parameters	12766/0/721	13166/0/549	2993/0/338	9732/2/428
Goodness–of–fit on F^2	1.059	1.019	1.231	1.088
Final R indexes [I>=2σ(I)]	R_1=0.0260, wR_2=0.0602	R_1=0.0773, wR_2=0.1084	R_1=0.0434, wR_2=0.1203	R_1 = 0.0388, wR_2 = 0.0775
Final R indexes [all data]	R_1=0.0343, wR_2=0.0641	R_1=0.771, wR_2=0.1196	R_1=0.0491, wR_2=0.124	R_1 = 0.0521, wR_2 = 0.0831

Table 3. Selected bond distances (Å) and angles (°) for $C_{50}H_{38}F_3NO_3P_2Ru$**(1a)**

Ru1 −P1	2.375(3)	N1 −Ru1 −P2	87.53	C14 −R1 −C1	90.90(5)
Ru1 −P2	2.410(3)	N1 −Ru1 −O2	88.22(4)	C33 −P1 −Ru1	117.66(4)
Ru1 −O2	2.195(9)	C1 −Ru1 −P1	89.20(3)	C39 −P1 −Ru1	116.64(4)
Ru1 −N1	2.152(11)	C1 −Ru1 −P2	89.61(3)	C45 −P1 −Ru1	113.06(4)
Ru1 −C1	2.043(12)	C1 −Ru1 −O2	166.52(4)	C15 −P2 −Ru1	116.69(4)
Ru1 −C14	1.845(13)	C1 −Ru1 −N1	78.94(5)	C21 −P2 −Ru1	119.49(4)
P1 −Ru1 −P2	178.806(1)	C14 −Ru1 −P1	88.72(4)	C27 −P2 −Ru1	113.09(4)
O2 −Ru1 −P1	87.23(3)	C14 −Ru1 −P2	91.19(4)	C7 −N1 −Ru1	114.36(8)
O2 −Ru1 −P2	93.95(3)	C14 −Ru1 −O2	102.00(5)	C11 −N1 −Ru1	126.19(9)
N1 −Ru1 −P1	92.35(3)	C14 −Ru1 −N1	169.76(5)	C2 −C1 −Ru1	128.58(10)
C6 −C1 −Ru1	114.93(9)	O1 −C14 −Ru1	174.62(12)		

Table 4 Selected bond distances (Å) and angles (°) for $C_{51}H_{40}F_3NO_3P_2Ru$ **(1b)**

Ru1 −P2	2.419(6)	N1 −Ru1 −O2	88.24(7)	C37 −P2 −Ru1	113.06(7)
Ru1 −P1	2.375(6)	C11 −Ru1 −P2	88.90(6)	C43 −P2 −Ru1	120.07(8)
Ru1 −O2	2.201(16)	C11 −Ru1 −P1	88.52(6)	C13 −P1 −Ru1	117.69(7)
Ru1 −N1	2.153(18)	C11 −Ru1 −O2	166.60(7)	C19 −P1 −Ru1	112.83(7)
Ru1 −C11	2.036(2)	C11 −Ru1 −N1	78.98(8)	C25 −P1 −Ru1	116.82(7)
Ru1 −C49	1.847(2)	C49 −Ru1 −P2	92.01(7)	C50 −O2 −Ru1	125.85(15)
P1 −Ru1 −P2	177.37(2)	C49 −Ru1 −P1	87.52(7)	C1 −N1 −Ru1	126.09(16)
O2 −Ru1 −P2	94.49(4)	C49 −Ru1 −O2	102.12(8)	C5 −N1 −Ru1	114.33(15)
O2 −Ru1 −P1	88.14(4)	C49 −Ru1 −N1	169.64(9)	C6 −C11 −Ru1	115.07(16)
N1 −Ru1 −P2	86.97(5)	C49 −Ru1 −C11	90.70(9)	C10 −C11 −Ru1	128.44(17)
N1 −Ru1 −P1	93.02(5)	C31 −P2 −Ru1	115.83(7)		

Table 5. Selected bond distances (Å) and angles (°) for $C_{22}H_{22}F_6O_6P_2Ru$ **(2)**

Ru1 −P1	2.380(13)	O5 −Ru1 −P2	85.44(10)	C9 −P1 −Ru1	111.56(16)
Ru1 −P2	2.379(13)	C1 −Ru1 −P1	90.68(15)	C15 −P2 −Ru1	110.96(18)
Ru1 −O3	2.101(3)	C1 −Ru1 −P2	92.94(15)	C16 −P2 −Ru1	115.57(19)
Ru1 −O5	2.101(3)	C1 −Ru1 −O3	174.33(18)	C3 −O3 −Ru1	123.4(3)
Ru1 −C1	1.864(5)	C1 −Ru1 −C2	87.6(2)	C5 −O5 −Ru1	122.1(3)
Ru1 −C2	1.889(5)	C2 −Ru1 −P1	90.67(15)	O1 −C1 −Ru1	176.0(4)
P2 −Ru1 −P1	176.38(5)	C2 −Ru1 −P2	89.40(15)	O2 −C2 −Ru1	174.2(5)
O3 −Ru1 −P1	87.56(10)	C2 −Ru1 −O3	176.33(18)		
O3 −Ru1 −P2	92.16(10)	C2 −Ru1 −O5	97.11(18)		
O3 −Ru1 −O5	79.71(13)	C7 −P1 −Ru1	115.53(19)		
O5 −Ru1 −P1	90.96(10)	C8 −P1 −Ru1	113.08(18)		

Table 6. Selected bond distances (Å) and angles (°) for $C_{29}H_{30}F_9N_2O_3P_3Ru$ **(3a)**

Ru1 −P1	2.37(12)	N1 −Ru1 −P2	89.29(11)	C15 −P1 −Ru1	111.75(18)
Ru1 −P2	2.37(12)	N1 −Ru1 −O2	168.30(15)	C16 −P1 −Ru1	111.24(15)
Ru1 −O2	2.08(3)	N1 −Ru1 −N2	78.61(15)	C22—P2 Ru1	115.75(19)
Ru1 −N1	2.05(4)	N2 −Ru1 −P1	86.65(11)	C23 −P2 −Ru1	116.04(17)
Ru1 −N2	2.10(4)	N2 −Ru1 −P2	89.51(11)	C24 −P2 −Ru1	111.95(15)
Ru −C1	1.86(5)	C1 −Ru1 −P1	93.21(15)	C12 −O2 −Ru1	123.6(3)
P1 −Ru1 −P2	175.49(6)	C1 −Ru1 −P2	90.86(15)	C2 −N1 −Ru1	125.7(3)
O2 −Ru1 −P1	86.30(10)	C1 −Ru1 −O2	96.46(18)	C6 −N1 −Ru1	116.1(3)
O2 −Ru1 −P2	91.33(10)	C1 −Ru1 −N1	95.22(18)	C7 −N2 −Ru1	114.6(3)
O2 −Ru1 −N2	89.71(14)	C1 −Ru1 −N2	173.81(19)	C11 −N2 −Ru1	125.8(3)
N1 −Ru1 −P1	92.25(11)	C14 −P1 −Ru1	118.16(18)	O1 −C1 −Ru1	176.2(4)

4.4. Electrochemistry

Redox properties of all ruthenium complexes were determined by cyclic voltammetry where Ag/AgCl was used as reference electrode. Behaviors of compounds were determined in 0.1M $[NBu_4^+PF_6^-]$/ CH_2Cl_2 solution with scan rate 50 mV/sec. The metal centered oxidation in both complexes involves the one electron transfer process. There is little shift in peak value for **1b** probably owing to the difference in electronic properties. Redox potential value for **1a** is slightly higher than **1b,** which is consistent with the electron deficient environment of complex **1a** relative to **1b**. The electron–donating effect of methyl group might destabilize the LUMO energy level and reveals its more electron efficient behavior.

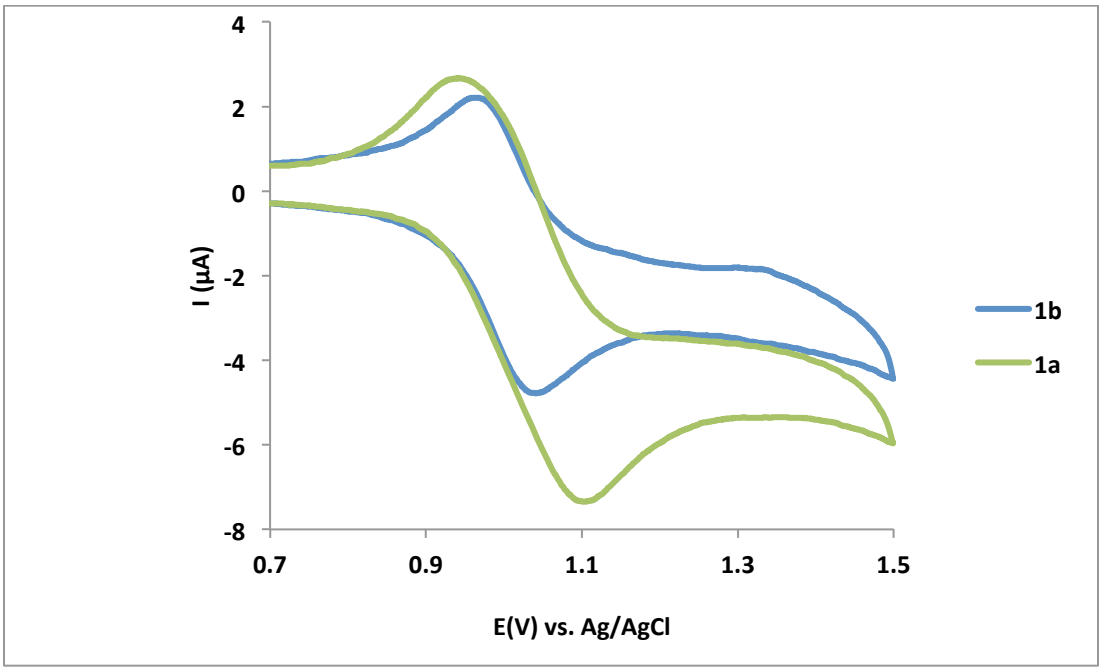

Fig. 9. CV of a 1.0 mM solution of **1a** and **1b** in CH_2Cl_2 containing 0.10 M$[NBu_4][PF_6]$, at a GC working electrode

In the bipyridyl–based complexes, (**3b** and **3c**), the cyclic voltammetry responses are not well resolved and show a number of ill–defined peaks. Stabilization of particular oxidation state is determined by the σ–donor and π–acceptor tendencies of surrounding ligands. Donor

properties of ligands always tend to stabilize Ru (III) over Ru (II) oxidation state while the π–acceptor ligands lead to the stabilization of Ru (II) state. Therefore, redox peaks appear in different potential ranges. For the complex, **3b** and **3c** only the redox behavior is quasi –reversible at potential E° = −2.87 V and E° = −3.12 V respectively while the others are irreversible. The difference in this redox value of two complexes can be understood in terms of electronic nature of bipyridyl ligands. Since the electron releasing tendency of 4,4′–dimethyl–2,2′–bipyridyl ligand is greater relative to the 2,2′–bipyridyl ligand and this increased electron rich environment in metal center might be responsible for the lower redox value for complex **3c**. There are other irreversible ill–resolved peaks on the complexes which might be caused by both metal–and ligand–centered reduction but it is difficult to specify on the basis of observed CV.

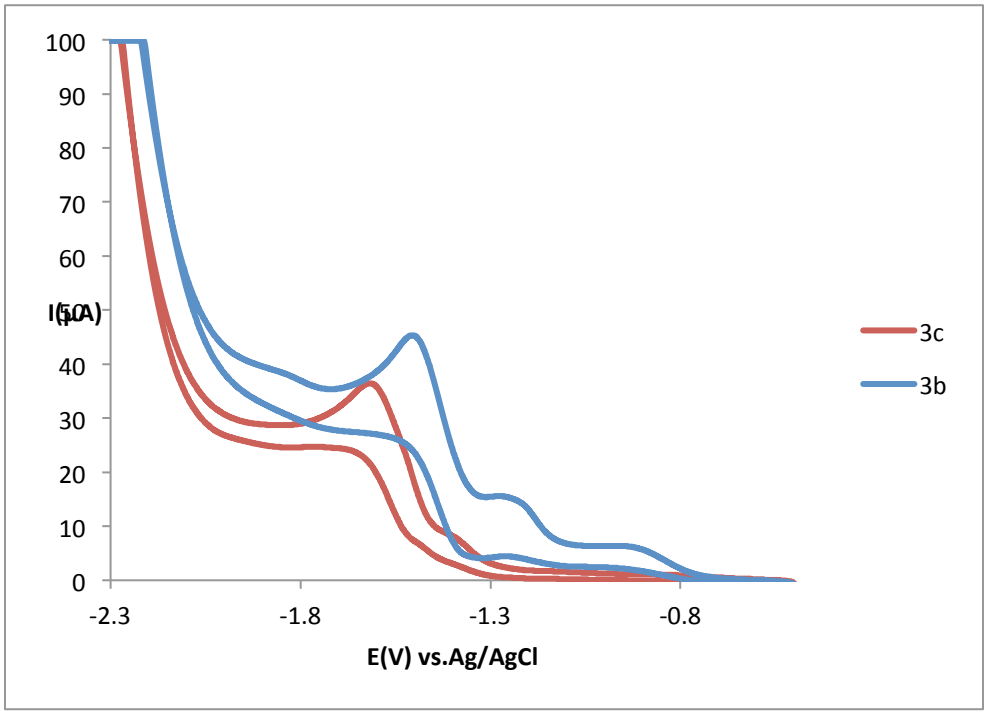

Fig. 10. CV of a 1.0 mM solution of **3b** and **3c** in CH_2Cl_2 containing 0.10 M$[NBu_4][PF_6]$, at a GC working electrode

The reduction potential value for Ru(II)–Ru(III) in both sets of complexes (**1a**, **1b**) and (**3b**, **3c**) should have some relation with σ–donor and π–acceptor tendencies of phosphine

ligands. Since the basicity of dimethylphenylphosphine is higher relative to triphenylphosphine, the ionic complexes (**3b** and **3c**) should oxidize easily than the complexes with triphenyl phosphine but the trend is just opposite [57]. Probably this opposite trend was resulted by higher sigma donor ability of cyclometallated ppy over the diimine bpy ligands.

Photophysical properties of complexes

5.1 Absorption Spectra

Absorption spectra of the Ru −complexes were measured at room temperature by using methylene chloride as solvent. Owing to its larger orbital size, ruthenium complexes acquires d^6 electronic configuration in its t_{2g} set of orbitals. On the other hand, ppy–R and bpy–R ligands have low lying π* orbitals that upon the excitation accepts an electron from metal center. Consequently, the complexes **1a** and **1b** show the weak and broad absorption band ranging from 385–450 nm because of single metal−to−ligand charge transfer (^{1}MLCT) (Table 7) from the electron-rich metal center. Similarly, the absorption bands around 280 nm exhibited a number of strong absorption bands which are attributed to π→π* charge–transfer transition.

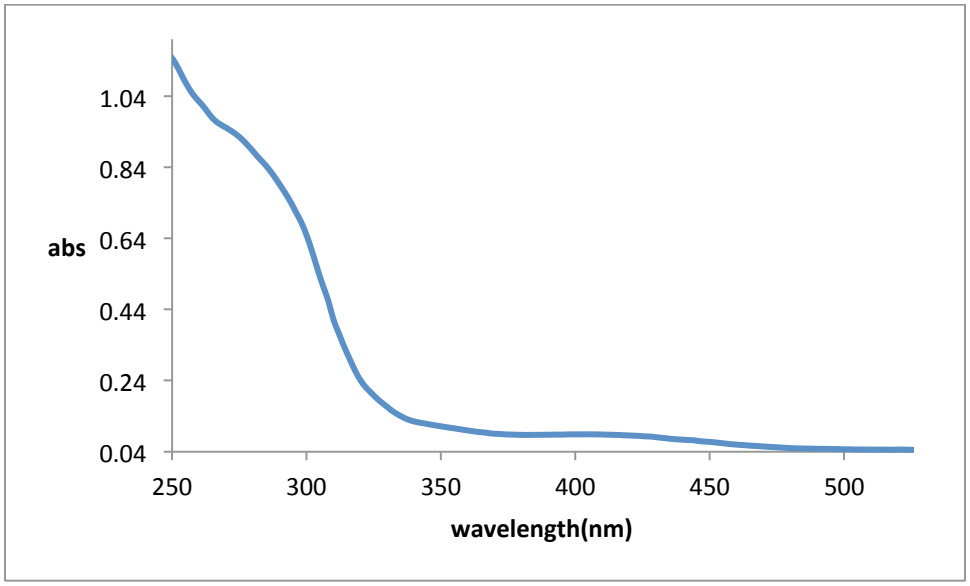

Fig. 11. Absorption spectra **1a** in methylene chloride

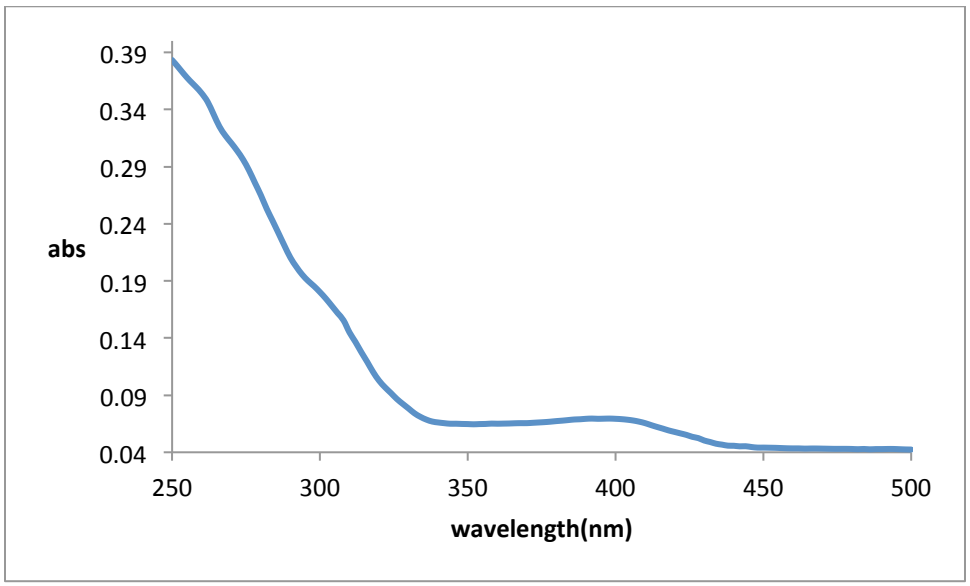

Fig. 12. Absorption spectra **1b** in methylene chloride

On the other hand, the diimine chelating complexes display the weak absorption bands between 450−500 nm due to the metal–to–ligand charge transfer (^{1}MLCT) and broad peak between 380−440 nm is assigned as ligand centered transition. In those complexes, strong absorption bands below 290 nm are assigned to the π→π* transition. Although both sets of ligands are analogous to each other, their little structural difference plays a vital role in their photochemistry. Since the cyclometallated anionic ppy–R ligand in **1a** and **1b** has strong σ–donating ability than their bpy–R counter parts (**3a**, **3b**, **3c**, **3d** and **3d′**), they increase the electron density surrounding the central Ru^{2+} ion and the ligand field strength as well [53].

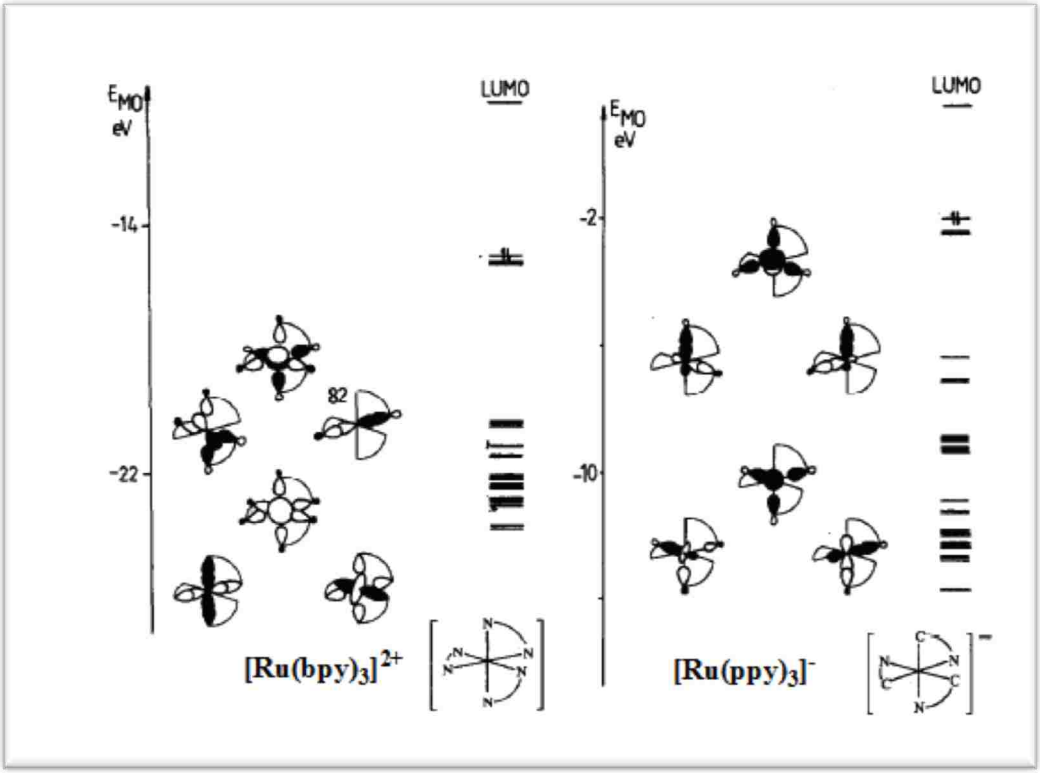

Fig. 13. MO diagrams of $[Ru(bpy)_3]^{2+}$ and $[Ru(ppy)_3]^{-}$ with their frontier orbitals [53].

The differences in photophysical properties of Ru-complexes with ppy-R ligand (**1a**, **1b**) and bpy-R ligands (**3a**, **3b** and **3c**) can be interpreted by taking the reference of MO diagram of $[Ru(ppy)_3]^{-}$ and $[Ru(bpy)_3]^{+}$ as shown MO diagram, **fig. 13.** Although both complexes have D_3 symmetry, there are some structural differences in the nature of their frontier orbitals and thereby leading to the differences in their photophysical behavior [53].

The d–orbitals of ruthenium metal center and phenyl part of ppy–R ligand (**1a**, **1b**) build up HOMO whereas low lying pyridine π*–orbitals represent the LUMO of whole metal complex. Since d^6 orbitals of central metal are properly lined up with the HOMO of ppy–R ligand, HOMO energy level is significantly lowered by strong field ppy–R ligand thereby further increasing the

HOMO–LUMO energy gap. Consequently metal to ligand charge transfer (MLCT) transitions in these complexes occurs in shorter wavelength region and exhibit the hypsochromic shift [53].

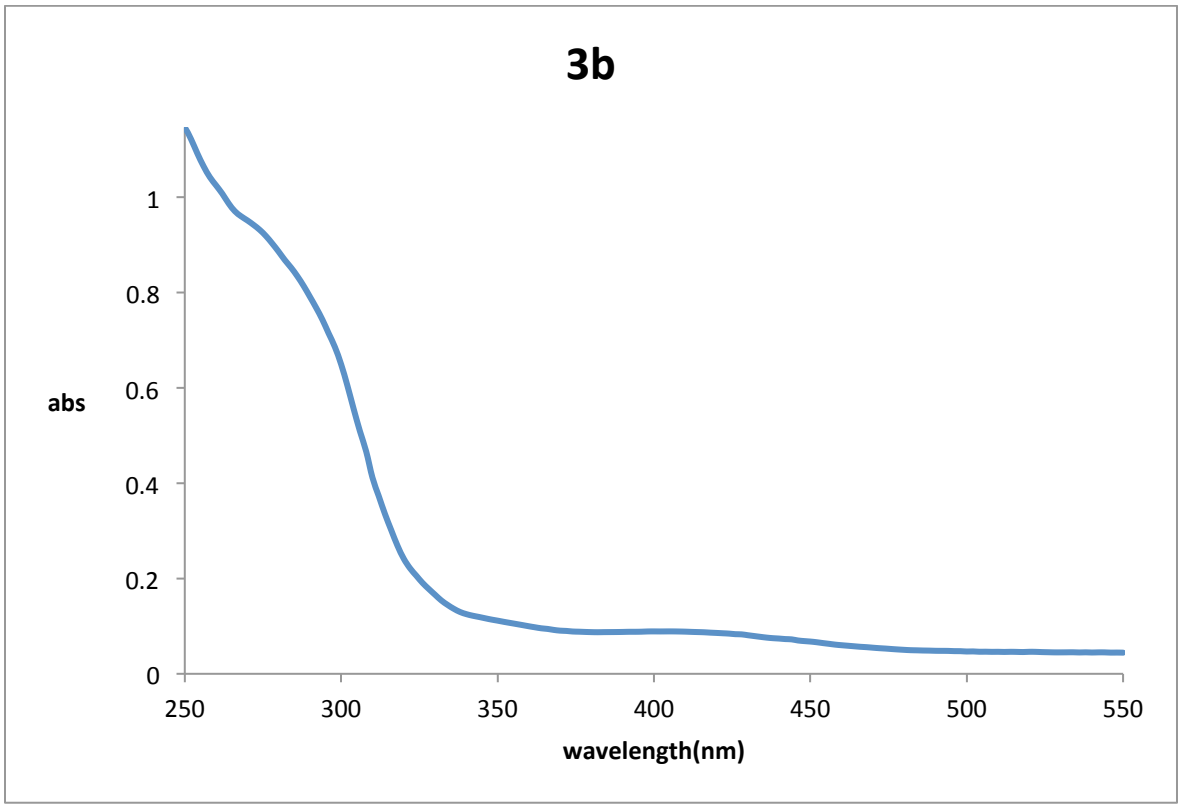

Figure 14: Absorption spectra **3b** in methylene chloride

On the other hand, in a series of **3a–3c** complexes, diimine bpy–R ligands have been used as luminophores. In terms of molecular orbital diagram, t_{2g} sets of d–electrons in Ru-center are involved in HOMO while both low–lying π*–orbitals on pyridyl rings in LUMO. Since the bipyridyl group is relatively weak field ligand, it occupies the lower position in the spectrochemical series. Due to the same reason, the magnitude of energy resulted by splitting of e_g and t_{2g} level is very low and thereby resulting the MLCT transition from low lying t_{2g} to excited π*-orbitals pyridine ring falls in bathochromic region [53].

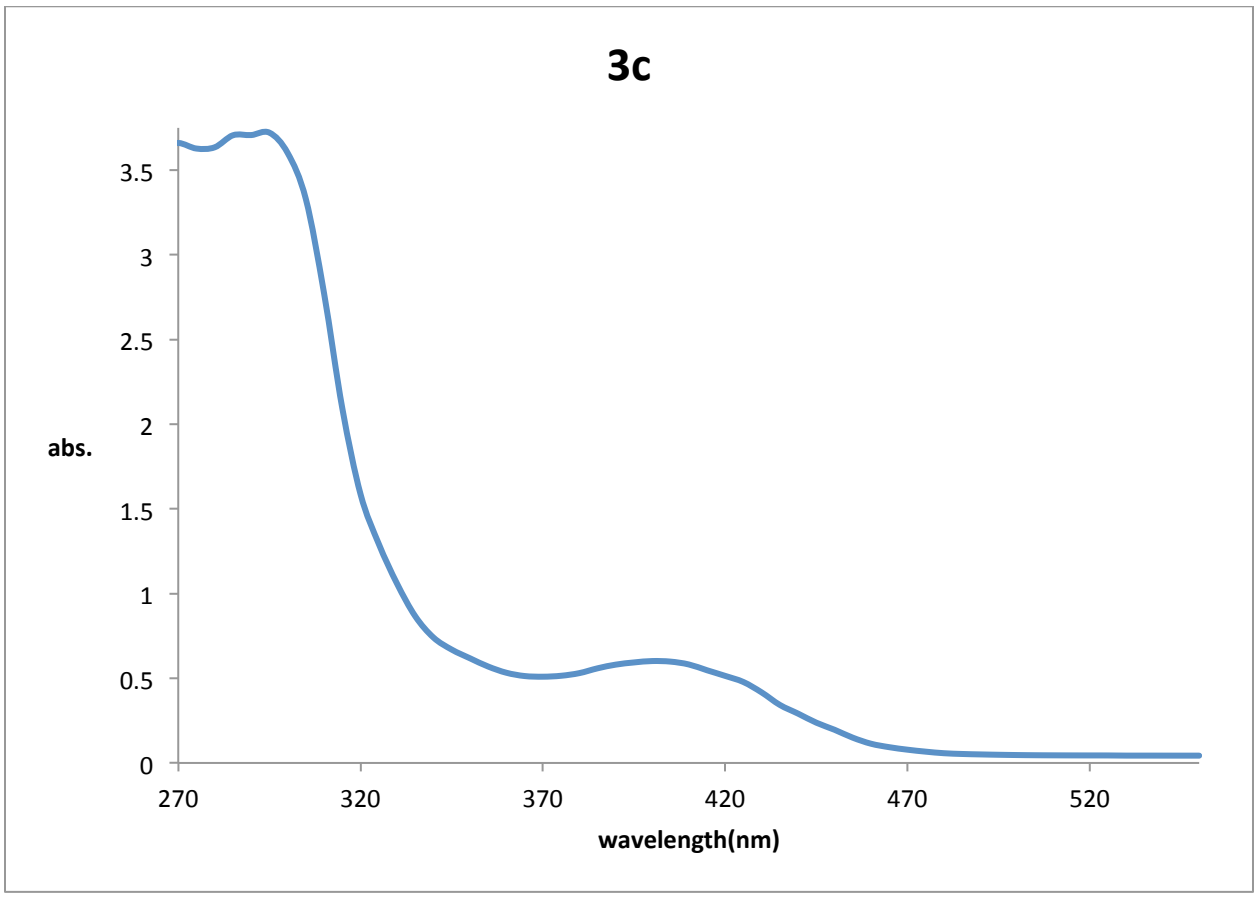

Fig. 15. Absorption spectra of **3c** in methylene chloride

In designing the two sets of Ru (II) complexes with ppy and bpy ligands, we carefully introduced the phosphine ligands. In the complexes **1a** and **1b**, there are two triphenylphosphine groups. They coordinated to the metal center as σ– donor and π– acceptor ligands and enhance the stability of HOMO energy level. Therefore, the complexes with PPh_3 ligands are supposed to have highly stabilized HOMO energy level and thereby absorbing radiation in higher energy region. On the other hand, complexes, **3a**, **3b** and **3c** have two dimethylphenylphosphine groups. They are coordinated to the Ru (II) center as a good σ–donors but very weak π–acceptors ligands. In general, this environment is responsible for the instability on metal center and thereby decreasing the HOMO–LUMO energy gap and shifting the MLCT transition at lower energy

region. [48]. However our experimental result could not show any significant differences in the photophysical behavior of complexes in either cases [28].

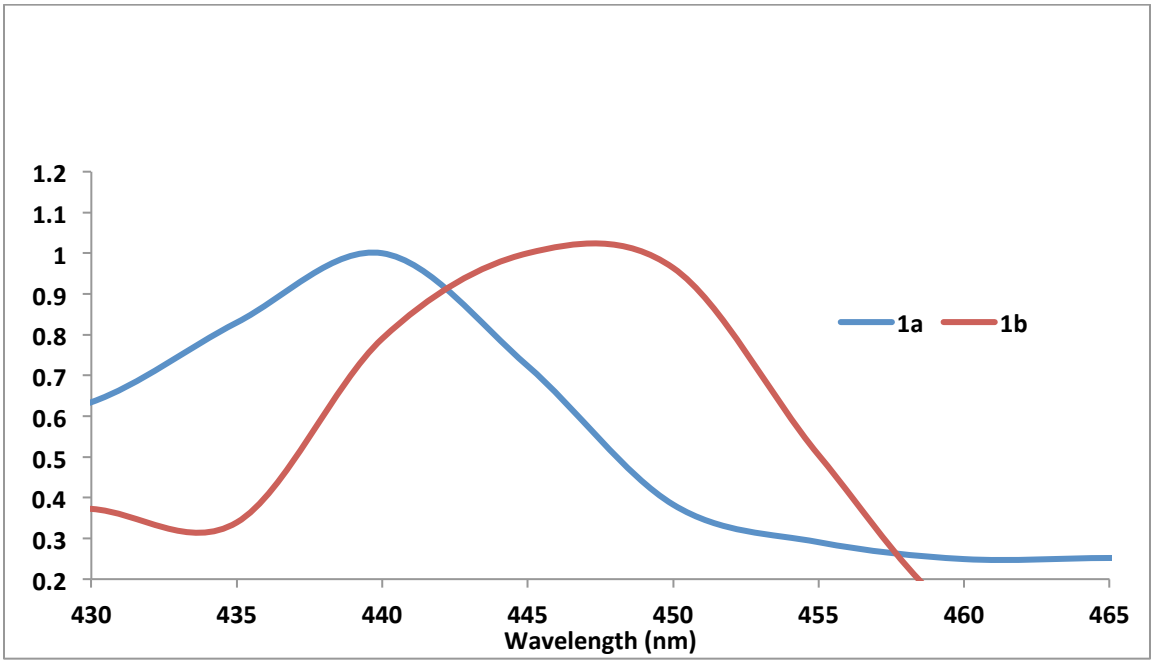

Fig. 16. Emission spectra **1a** and **1b** in methylene chloride

After the photophysical study of Ru (II) complexes with ppy and bpy ligands, we tried to measure the absorption wave length of brominated complexes **3d–3d′.** However those complexes did not exhibit any specific absorption on MLCT transition probably, due to the heavy atom–effect of bromine.

Table 7. UV–Vis absorption and emission data in DCM solution

Compound	λ_{abs} MLCT (nm)	λ_{exc}(nm)	λ_{e}(nm)	τ (ns)
1a	390	390	440	–
1b	400	400	450	–
3b	480	470	600	330
3c	480	470	610	270

5.2 Emission Spectra

Since ruthenium is a heavy metal, it facilitates the spin–orbit coupling. Therefore excited singlet state (^{1}MLCT) of its complexes easily undergoes intersystem crossing and emission originates from low lying triplet state (^{3}MLCT). All the luminescence data were recorded at room temperature in methylene chloride solution as shown in Table 7. The emission spectra of all complexes with bpy–R ligands (**3b – 3c**) are red–shifted relative to those with ppy–R ligands (**1a – 1b)**.

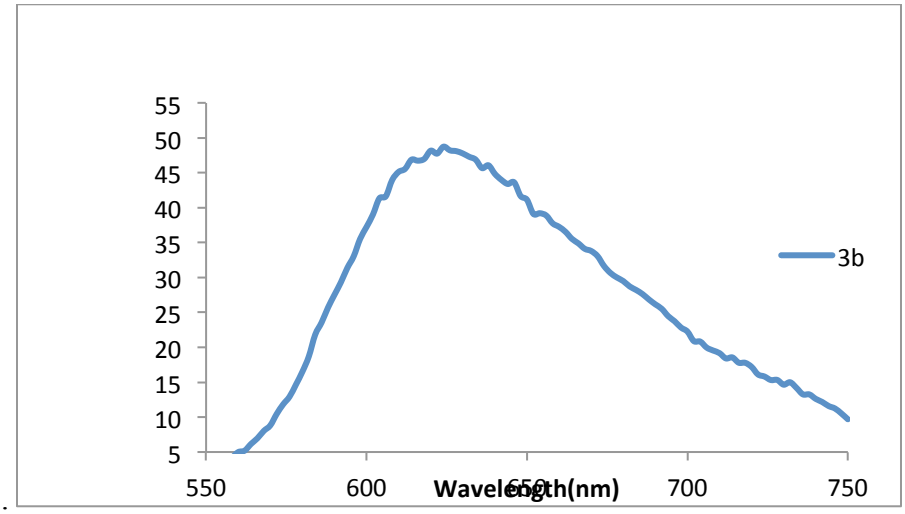

Fig.17. Emission spectra of **3c** in solution

Since there is a very weak MLCT charge transfer band for complexes with cyclometalated ppy–R ligands, they emit in very high energy region. However, the electron donating methyl group in complex **1b** is responsible for lowering the HOMO–LUMO energy gap, its emission appears at lower energy region in comparison to **1a**. Likewise, between **3b** and **3c**, the second one emits in lower energy (red–shifted) region. This might be resulted by the higher electron donating tendency of methyl groups in the 4,4′–position of 2,2′–bipyridyl ligand. Since complexes **1a** and **1b** exhibit blue–shifted emission we did not measure the lifetime but complexes **3b** and **3c** are have longer lifetime *viz.* 330 and 270 ns respectively. From the excitation spectra of complex **3c** (Fig. 17), it is obvious that the major contribution to the excited state comes from the MLCT absorption band.

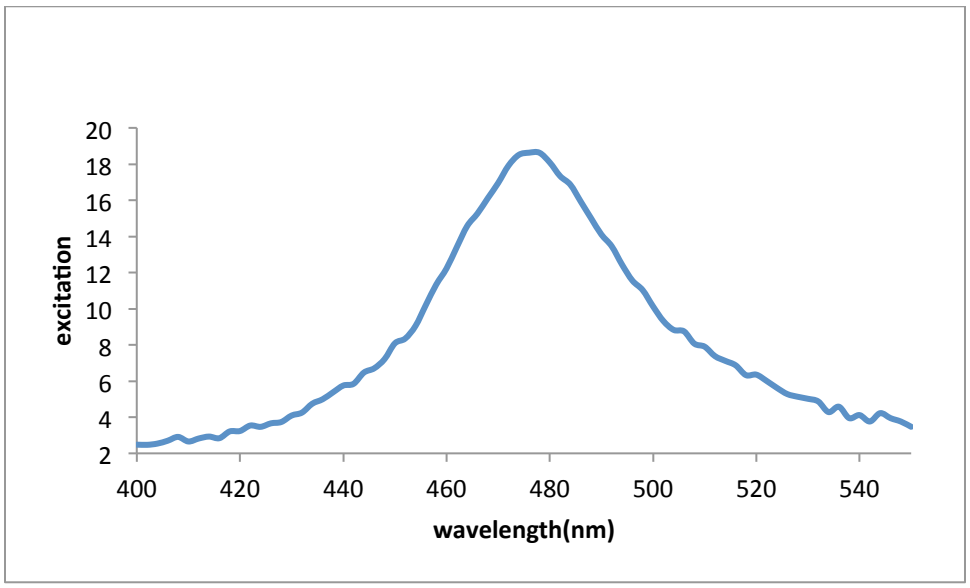

Fig. 18. Excitation spectra of complex **3c**

6. Conclusion:

We synthesized 2,2'-bpy and ppy-complexes of Ru(II) with the intention of introducing a tethering group on ligand to conjugate the complexes with silica polyamine composites. These complexes were characterized by spectroscopic studies as well as X-ray crystallography before their loading with SPC. The redox behavior of the complexes were studied by cyclic voltammetry and found that the bpy-R complexes of Ru(II), in general, exhibited irreversible wave whereas the ppy-R complexes showed pseudoreversible wave. The photophysical properties of the complexes revealed that the bpy-R complexes of Ru(II) showed red-shifted emission in comparison to the ppy-R complexes. We introduced monobromo group to 4,4-dimethyl-2,2-bipyridyl ligand before its complexation with the metal center. That bromo group

was used to conjugate the complex with silica polyamine composites, and the conjugation was studied by FT-IR spectroscopy. We observed better loading of the complex with bromo group to silica polyamine composite in comparison to amine, carboxylic acid and aldehyde functional groups studied by Abbott, et al. [33]. We also studied the effects of size on ancillary phosphine ligand in turning luminescence of the complexes and their loading in SPC. Within the same environment, the Ru(II) complexes with 2,2′–bipyridyl ligands have shown the bathochromic behavior while those with 2–phenylpyridyl ligands have shown hypsochromic shifts. Although we had expected the red-shifted absorption-emission spectra after the modification of ancillary phosphine ligands, there were no significant changes in their luminescent behavior [28].

Future Work

In this work we have successfully synthesized and characterized some ruthenium complexes with cyclometallated ppy-R ligand (**1a** and **1b**) and chelating bpy-R ligands (**3a** and **3b**). Although we have measured the absorption-emission wavelength of **3a** and **3b** along with their excited state lifetime, we have not been able to measure the quantum yields of these compounds.

We also have synthesized the diimine ruthenium complex after the bromination of one of the methyl group on 4,4′–dimethyl–2,2′–bipyridyl ligand (**3d** and **3d′**) and loaded them on Silica polyamine Composite (BP–1). Although we have performed some preliminary studies characterizing the loading of complexes on silica surface by IR, full characterization using ^{13}C NMR, solid state ^{31}P NMR and microanalysis have not been done so far. Measurement of excitation and emission wavelength as well as measurement of excited-state-lifetime of silica-bound complexes gives some idea of their suitability for carrying photochemical reactions as heterogeneous catalysis.

Bibliography

1. K. Kalyanasundaram, M. Gratzel, *Coord. Chem. Rev*., **177** (1998), p. 347.
2. D.P. Rillema, G. Allen, T.J. Meyer and D. Conrad, *inorg. Chem.,* **22** (1983), p.1617.
3. P.Wang, S,M. Zajeeruddin, J.E. Moser, M.K.Nazeeruddin, T. Sekiguchi and M. Gratzel, *Nat. Mater.,* **2** (2003), p.402.
4. M. Gratzel, *Inorg. Chem*., **44** (2005), p.6841.
5. I. Bedja, S. Hotchandani, and P.V. Kamat, *J. Phys.Chem,* **98** (1994), p.4133.
6. M. Kimura. M. Yamashita and S. Nishida, *Inorg. Chem,* **24** (1985), p.1527.
7. J. K.Hurst, J.L. Cape, A.E. Clark, S. Das and C. Qin, *Inorg. Chem.* **47** (2008), p.1753.
8. J. Xie, C. Li, Q. Jhou, W. Wang, Y. Hou, B. Jhang and X. Wang, *Inorg. Chem*. **51** (2012), p.6376.
9. C. Malins, H.G. Glever, T.E. Keyes, J. G. Vos, W.J. Dressick and B.D. MacCraith, *Sens. Actuators, A*., **67** (2000), p.89.
10. M. K. Nazeeruddin, D. D. Censo, R. Hamphry −Baker and M. Gratzel, *Adv. Funct. Mater,* **16** (2006), p.189.
11. E. Berni, I. Gosse, D. Badocco, P. Pastore, N. Sojic and S. Pinet, *Chem. Euro. J.,* **15** (2009) p.5145.
12. M.P. Pyle, J.P. Rehmann, R. Meshoyrer, C.V. Kumar, N.J. Turro and J.K. Barton, *J. Am. Chem. Soc.,* **111** (1989) p.3051.
13. A. Sharmin, L. Salassa, E. Rosenberg, J.B.A. Ross, G. Abbott, L. Black, M. Terwilliger, R.Brooks, Inorg. Chem., **52** (2013), p.10835.
14. K. Berggren, E. Chernokalskaya, T.H.Stainberg, C. Kemper, M.F. Lopez, Z. Diwu, R.P. Haugland and W.F. Patton, *Electrophorosis*, **21** (2000), p.2509.
15. L.E. Orgel, *Chem. Soc.*,(1961), p.3683.
16. E.M. Kober, B.P. Sullivan and T.J. Meyer, *Inorg. Chem.,* **23** (1984), p. 2098.
17. G.A. Crosby, *Acc. Chem. Rev*, **8** (1975), p.231.
18. G.A. Crosby, *Adv. Chem. Ser.,* **150** (1976), p. 149.
19. E.M. Kober and T.J. Meyer, *Inorg. Chem.,* **21** (1982), p.3967.

20. K. Mandal, T.L.D. Pearson, W.P. Krug and J.N. Demas, *J. Am. Chem. Soc.,* **105** (1983), p.701.
21. K. Kalyanasundaram, *Coord. Chem. Rev.,* **46** (1982), p.159.
22. E.A. Seddon and K.R. Seddon, *The Chemistry of Ruthenium*, (1984), Elsevier, New York.
23. R.J. Watts, *J.Chem Educ.,* **60** (1983), p. 834.
24. A. Juris, V. Baljani, F. Barigelletti, S. Campagna, P. Belser and A. Von Zelewsky, *Coord. Chem. Rev*., **84** (1988), p.85.
25. V. Balzani, A. Juris, M. Ventury, S. Campagna and S. Serroni, *Chem. Rev*., **96** (1996), p.759.
26. D. Felder, J.F. Nierengarten, F. Barigelletti, B. Ventura and N. Armaroli, *J. Am. Chem. Soc.,* **123** (2001) , p.6291.
27. G.A. Grosby, R.J.Watts and D.H. W. Carstens, *Science,* **170** (1970), p.1195.
28. A. Sharmin, R. C. Darlington, K.I. Hardcastle, M. Ravera, E. Rosengerg and J.B. A. Ross, *J. Organomet. Chem.* **694** (2009), p.988.
29. E.C. Constable and C.E. Housecroft, *Polyhedron*, **9** (1990), p.1939.
30. M.A. Hughes and E. Rosenberg, *Sep. Sci. Technol*. **42** (2007), p.261.
31. R.J. Fischer, D. Pang, S.T. Beatty and E. Rosenberg, *Separ. Sci. Technol*. **34** (1999), p. 2723
32. **.** Allen, E. Rosenberg, E. Karakhanov, S.V. Kardashev, A. Maxinov and A. Zolotukhina, *Appl. Organometal. Chem.* **25** (2011), p.245**.**
33. G. Abbott, R. Brooks, E. Rosenberg, M. Terwilliger, J.B.A. Ross and O.O.L. Ichire, *Organometallics*, **33** (2014), p.2467.
34. C. Garino, S. Ghiani, R. Gobetto, C. Nervi, L. Salassa, R. Rosenberg, J.B.A. Ross, Xi Chu, K.I. Hardcastle and C. Sabatini, *Inorg. Chem*., **46** (2007), p. 8752.
35. O.V. Borisov, D.M. Coleman, K. A. Oudsema and R.O. Carter III, *J. Anal. At. Spectrom*., **12** (1997), p.239.
36. C. A. Parker, Photoluminescence of Solutions with Application to Photochemistry and Analytical Chemistry, Elsevier, Amsterdam (1968), p. 262.
37. J. R. Lakowicz, Principles of Fluorescence Spectroscopy (3rd ed.), (2006), Springer, New York.

38. A.S. Minazzo, R.C. Darlington and J.B.A. Ross, *Biophys. J.,* **96** (2009), p.681.
39. M.L. Johnson and S.G. Frasier, In Methods Enzymol , Academic Press:, New York, (1985), p.301.
40. G.M. Sheldrick, (2001), SADABS: Area Detector Absorption Correction, University of Gottingen, Germany.
41. O.V. Dolomanov, L.j. Gildea, J.A.K. Howard and S.Puschmann, *J. Appl. Cryst.,* **42** (2009), p.339.
42. Bruker (2007), APEX2, Bruker AXS Inc., Madison, Wisconsin, USA.
43. G.M. Sheldrick, A short history of SHELX(2008). Acta. Cryst., **64** (2008), p.112.
44. M. Kercher, B. Koenig, H. Zieg, D.C.L. Herald, *J. Am. Chem. Soc.*, **124** (2002), p.11541
45. S. Gould, G.F. Strouse, T.J. Meyer and B.P. Sulivan, *Inorg. Chem,* **30** (1991), p.2942.
46. S.H. Lai, J.w. Ling, Y.M. Haung, M.J. Haung, C.H. Cheng and I.C. Chen, *J. Raman Spectrosc*., **42** (2011), p. 332.
47. F.A. Cotton, *Inorg. Chem*., **3** (1964), p. 702.
48. K.C. Hwang, J.L. Chen and Y. Chi, *Inorg. Chem.,* **47** (2008), p.3307.
49. D.A. Cavarzan, C.B. Pinheiro, M.P.D. Araujo, *Transition Met. Chem*., **40** (2015), p. 117.
50. S.O. Grim, D.A. Wheatland and W. McFarlane, *J. Am. Chem. Soc*., **89** (1967), p. 5573.
51. A.M. Clark, C.E.F. Rickard, W.R. Roper and L.J.Wright, *Organometallics*, **18** (1999), p.2813.
52. M.S. Eum, C.S. Chin, S.Y. Kim, C. Kim, S.K. Kang, N.H. Hur, J.H. Seo, G.Y. Kim and Y.K. Kim, *Inorg. Chem.,* **47** (2008), p.6289.
53. E.C. Constable and C.E. Housecroft, *Polyhedron*, **9** (1990), p. 1939.
54. B. Carlson, G.D. Phelan, J. Benedict, W. Kaminsky, K, Dalton, *Inorg.Chim. Acta.,* **357** (2004), p.3967.
55. G. Croce, M. Milanesio, D. Viterbo. C. arino, R.Gobetto, C. Nervi and L. Salassa, *CR Chim*., **8** (2005), p.1676.
56. C. Garino, T. Ruiu, L. Salassa, A. Albertino, C.Volpi and C.Nervi, Eur. *J Inorg. Chem.,* **23**(2008), p.3587.
57. B..P. Sullivan, D.J. Salmon and T.J. Meyer, *Inorg. Chem*., **17** (1978), p.3334.

Appendix

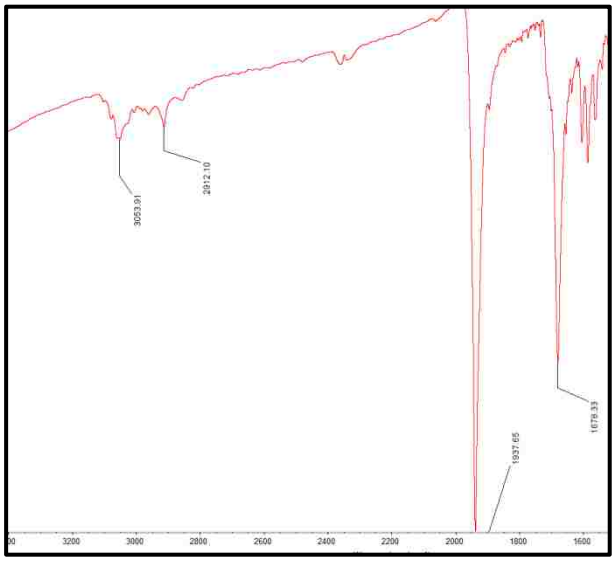

IR Spectra of **1b**

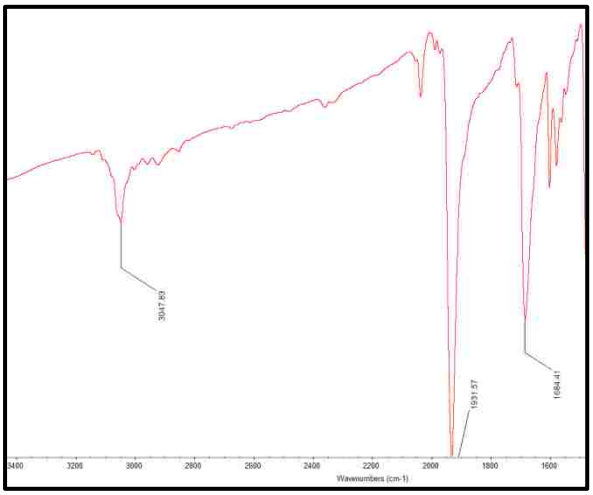

IR Spectra of **1a**

IR Spectra of **3a**

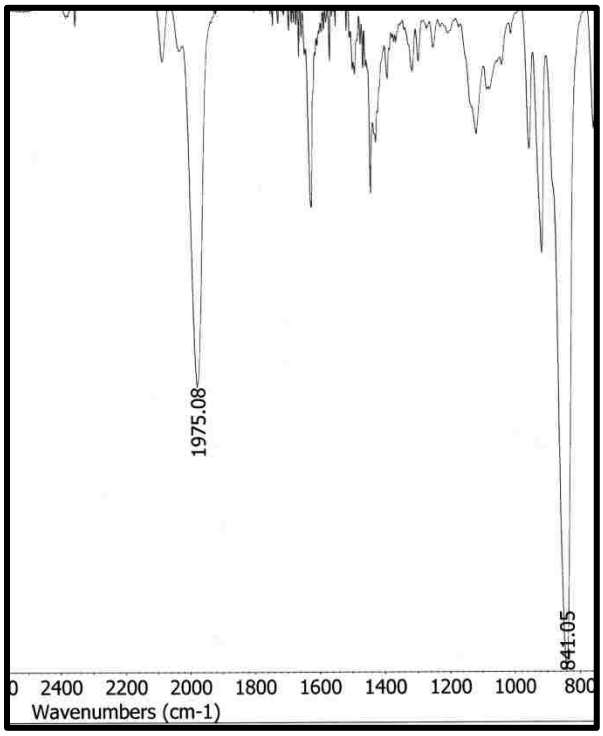

IR Spectra of **3c**

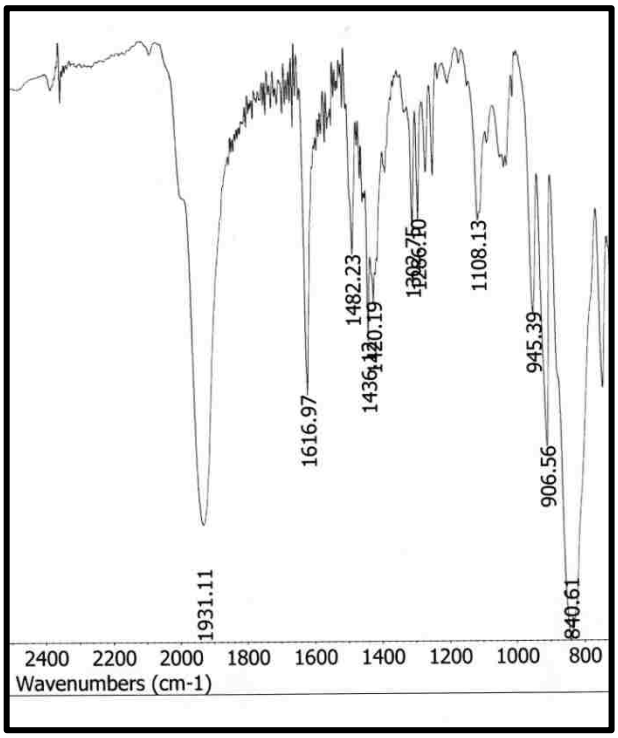

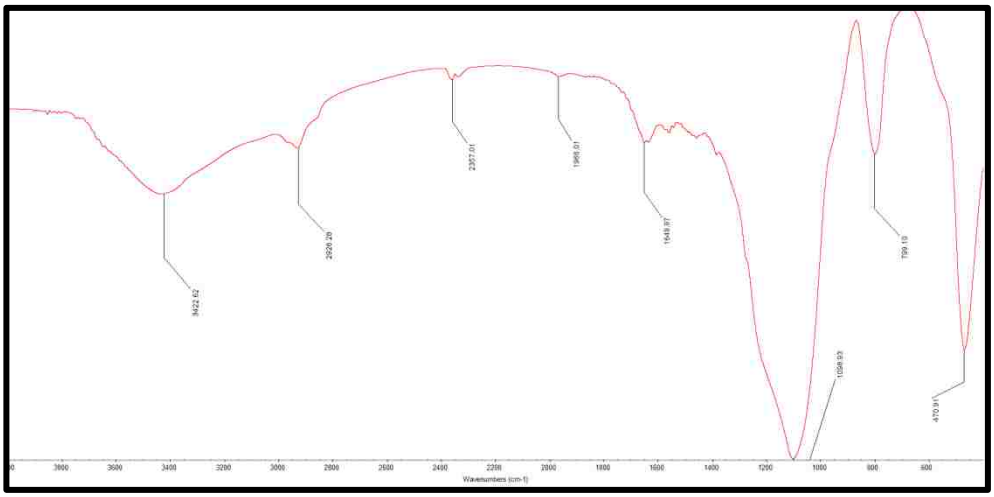
3422.62
2926.29
2357.01
1968.01
1649.87
1058.93
799.10
470.91
Wavenumbers (cm-1)

IR of Ru −SPC

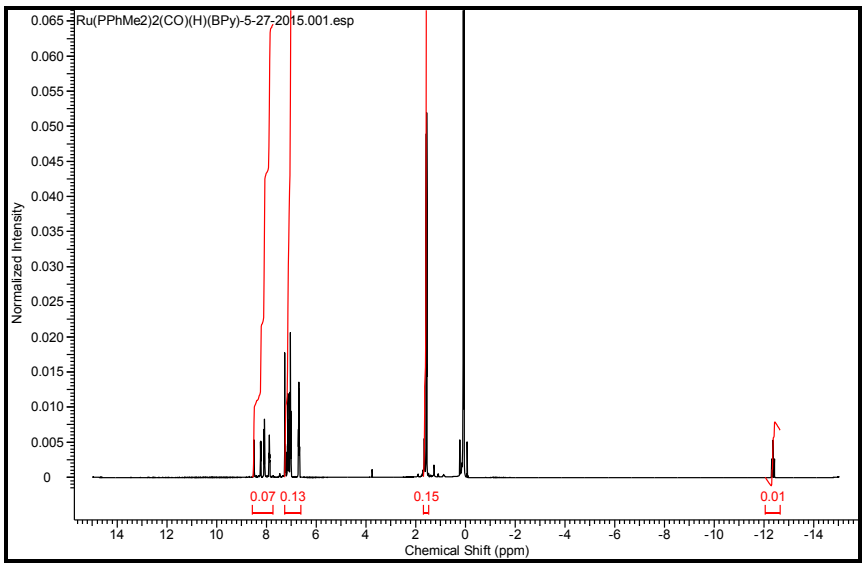

1H NMR of **3b**

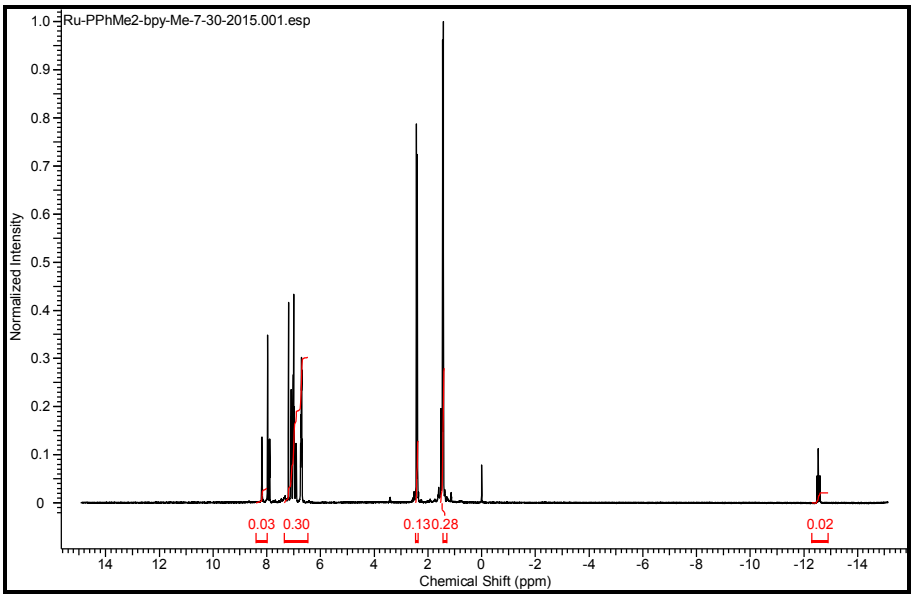

^{1}H NMR of **3c**